POSITIONAL ESTIMATION OF SOFT ACTUATORS THROUGH EMBEDDED SENSING

A Thesis
Presented to
The Academic Faculty

by

Alexander M. Hart

In Partial Fulfillment
of the Requirements for the Degree
Master of Science in the
George W. Woodruff School of Mechanical Engineering

Georgia Institute of Technology
May 2018

POSITIONAL ESTIMATION OF SOFT ACTUATORS THROUGH EMBEDDED SENSING

Approved by:

Dr. Frank Hammond III, Advisor
School of Mechanical/Biomedical Engineering
Georgia Institute of Technology

Dr. Dennis Dorozhkin
School of Mechanical Engineering
Georgia Institute of Technology

Dr. Jun Ueda
School of Mechanical Engineering
Georgia Institute of Technology

Date Approved: [February 01, 2018]

To Maverick

ACKNOWLEDGEMENTS

Graduate school in pursuit of a Master's degree has been my greatest endeavor to date. In two and a half years I faced challenging trials through academic study, research of an emerging field, and in my personal life as a young adult. In this accomplishment, I owe sincere gratitude to those who aided me in my struggles and guided me towards my ultimate goal. The wisdom and investment from others was paramount to my success.

Thank you to my mother, Shirley Hart, and father, Anthony Hart. A substantial challenge of my studies was the maintenance of my health and daily routines. You both were regularly available for consultation on these personal qualms. Mom, your advice in preparing food and watching my diet is incredibly beneficial. Thank you for the help with my taxes as well. Dad, thank you for the sound council you provide when I find myself at a personal crossroads. I am always listening.

Thank you to the Principle Investigator of my research, Dr. Frank Hammond III. Frank shares extensive knowledge of technique and theory in the field of soft robotics with those who pursue research in the Adaptive Robotic Manipulation Lab. He provided critical insight in choosing the scope of my research and guidance at every stage of its development. His expertise facilitated the advancement of my research and his professional mentorship taught me essential lessons in functioning efficiently as part of a multidisciplinary team. You were incredibly generous with your time and attention. Thank you for this immense opportunity to conduct research.

Thank you to my colleagues in research. We engaged in numerous collaborations and shared techniques for mutual understanding. Working in your proximity and recognizing admirations in your methods helped me identify substantial opportunity for my growth as an engineer. It was a pleasure to share this experience in academia with all of you and I hope that our careers cross path in the future.

Thank you to my canine companion, Maverick. The day in day out hardships I faced pushed me to great emotional lengths that were put into perspective by the simple ritual that we share and continue to share. Your company is enormously valuable to me.

TABLE OF CONTENTS

LIST OF TABLES

LIST OF FIGURES

LIST OF SYMBOLS AND ABBREVIATIONS

AGA	Adaptive Grasp Appendage
EGaIn	Eutectic Gallium Indium
FEA	Finite Element Analysis
HRI	Human Robot Interaction
LED	Light Emitting Diode
PAM	Pneumatic Artificial Muscle
SMA	Shape Memory Alloy

SUMMARY

Soft robotic systems are prone to deforming in undesired modes due to the compliant materials used to fabricate them. These systems often use pneumatic soft actuators that utilize internal pressure to induce constrained deformations. Controlling soft actuators partially requires system modeling, specifically in complex systems of multiple actuators. Acquiring accurate models through analytical methods, computational or manual, is challenging due to embedded components constraining elastic deformations of the body. Another approach to this challenge is observing system parameters through integrated sensing to develop an estimated model. As packaged soft sensing components are limited, research and development of the physical sensor and technique for implementation is required. Developing these methods involves mechanical design of components, electronic instrumentation, orientation and placement for target deformations, interpretation of response for embedded control, and benchmarking performance. The documentation of these attempts at sensor development serves to expand the toolbox of techniques for sensing in soft robotic bodies.

This thesis presents two approaches to the process. The first approach involved embedding conductive fluidic strain sensors in a bidirectional soft actuator of an assistive grasp prosthetic to characterize the undesired modes of deformation it experienced. Sensors were placed to observe the intended mode of bending as well as undesired lateral sag and rotational twist of the actuator body. These sensors provided haptic feedback of actuator position that enabled users to correctly identify grasp in 83.3% of responses. The second approach was the design and fabrication of a soft robotic grasp prosthetic incorporating control from embedded positional sensing. The primary grasping actuators were deployed

with an embedded fiber optic array monitoring reflectance against an internal diaphragm, capable of monitoring actuator tip position to an accuracy of 1.7mm. These sensor embedded actuators were employed in feedback control to independently alter grasp configuration to objects of varying shapes. From the studies it is evident that observation of specific actuator deformations are critical to determine sensor placement.

CHAPTER 1. **INTRODUCTION**

With the current field of soft robotics, the task of closed loop kinematic control is a substantial challenge. Soft robotic bodies, often composed of silicone or other elastic polymers, are difficult to characterize by discreet degrees of freedom. In the context of control, this impedes kinematic modeling of a soft robot. In general, soft robots can adapt to operational uncertainty without a need for accurate modeling through their natural compliance [1]. Despite this capability, soft robots would be applicable to a wider range of tasks if methods to better characterize a kinematic model were developed. For robots navigating through tight spaces, potentially search and rescue or surgical applications, a strong understanding of the physical configuration of the robot would likely benefit the system. There are some specific approaches to tackling this challenge. Analytical methods such as finite element analysis have been used to effectively model soft actuators for the response to specific loadings, but demand rigorous simulation [2],[3]. An alternative route is to utilize sensors in characterizing the deformations of silicone bodies [4],[5]. As modeling these systems proves to be a challenge, it is the author's belief that estimation based approaches from embedded sensing warrants exploration.

1.1 Soft Robotic Potential

Task-specific actuators are relatively simple to design and fabricate; armed with computer aided design and 3D-printing technologies, prototype actuator designs can be built relatively quick. A general workflow for the prototyping process of a soft actuator can be seen in Figure 1.

Figure 1- General workflow employed for soft actuator prototyping

The duration of design and modeling for soft components and molds is dependent on system complexity. 3D-printing and silicone casting are relative quick processes, allowing different configurations to be built and tested with ease, facilitating iterative design and experimentation.

The soft deformable texture of these systems facilitates our natural interaction with them. From an ergonomic perspective, physically interacting with another compliant body like our own should facilitate intuitive operation [6]. In terms of compliance matching, the polymers and materials that soft robotics are composed of are relatively close to our own flesh [7]. This quality gives soft robots a predisposition for healthcare, wearable devices, and any other field demanding extensive human robot interaction (HRI).

1.2 Soft Robotic Drawbacks

Soft robotic assemblies are subject to bully from the environments they operate in. In one study, a robot was subject to being run over by a car to successfully demonstrate its physically robust design [8]. Compliant materials that grant them such extensive adaptability simultaneously dooms them to a reactionary relationship with their environment. Habitual absorption of environmental disturbance takes its toll on the physical condition of the actuator along with the efficiency of its control. Spending energy to work through obstacles, as opposed to around them, is detrimental to the overall lifespan

of mechanical systems. While in most cases the expense is minor, soft robotics need precise kinematic control so that they may work smarter and not harder.

Soft robot design is open to much more creative freedom than traditional robots, and this actually poses a challenge. Compliant materials are less demanding to work with physically and 3D printing technology enables the fabrication of almost any geometry. A design process facilitated for rapid iteration allows the majority of actuators to be specific to the system task. Most cases of sensors being embedded in soft actuators approach the task in novel ways because the actuators are unique [4],[9],[10]. Compared to traditional robotics, where an encoder is used to measure the rotation of a shaft, there is not a broadly accepted method of for measuring the position of a soft actuator. Soft robotics have less structured protocols for establishing control of a system. Developing solutions to this problem means taking attempts at soft sensor integration in systems and determining their ultimate performance and the design aspects that allow them to succeed. In this way we hope to find optimal solutions for measuring principle modes of deformation experienced by soft actuators.

1.3 Outline

Chapter 2 is an overview of soft robotic technologies, actuators and sensors. This investigation is focused on the general configuration of pneumatic soft actuators and of a sensing methods potential to characterize the positional state of soft actuators.

Chapter 3 describes preliminary research done in adapting the actuators of an existing prosthetic with a soft sensing method. In this set of experiments, conductive

fluidic microchannels were embedded in a bidirectional pneumatic actuator to estimate the degree of bending, sagging, and twisting that the actuator underwent.

Chapter 4 corresponds to the development of a soft robotic prosthetic meant for grasp assistance. The system contains routed fiber optics to characterize actuator position for the purpose of achieving grasp synergies dependent on the shape of the object in grasp.

Chapter 5 reflects on the full scope of research conducted in this investigation. It addresses general observations on the performance of tested systems and aspects to improve. The contribution of the work to soft robotics as a field is defined and an aim for further research is given.

CHAPTER 2. STATE OF THE ART

2.1 Sensing for Soft Robotics

Soft robotic systems demand development of sensing methods and technique in order to help move the field in a practical direction. There have been significant advancements within the past decade in the direction of soft sensing solutions. Any sensing method deployed in a soft robotic system is subject to system specific criteria determined by the design of the actuator. These criteria range from general anticipated locations of deformation to specific embedded components that should be avoided or utilized for increasing accuracy of the sensor response.

Sensing in the body of a compliant system means assuming the sensing area can be subject to any feasible configuration of strain through it. The first order of concern is to minimize lasting physical effect on the sensor and region. In the minor case, hysteresis would be considered a substantial yet temporary physical ailment. A major physical ailment would be physical degradation of the sensor and its capability to measure. This may be exemplified by delamination of a sensing body from the surrounding body, thereby changing a positional reference. The second consideration is with how external disturbances to the actuator are effecting the response of embedded sensing. This could be physical force on the actuator, electromagnetic interference, or even optical interference in some sensing methods. Designing for these conditions is often accounted for in the design of a sensor and actuator based on predictions of how the elastic bodies will behave. Specifically with directional strain sensing, sensor bodies are placed with proper orientation so the sensor will react less to deformations it is misaligned to [11]. Until sensing methods are refined towards full understanding of the physical body, current

technologies operate on an assumption that the actuator is operating without anticipated disturbance to give a general estimation of the deformation. It is a goal of this research to reduce the impact of external disturbance of kinematic understanding of the body.

2.1.1 Conductive Fluidic Micro-Channels

Conductive fluidic micro-channels are a method of soft sensing that has been well documented and explored [12],[13],[14]. This process typically involves the fabrication of vacant channels within a body of silicone, followed by the injection of a conductive fluid, such as Eutectic Indium Gallium (EGaIn), throughout the channel, Figure 2 [15].

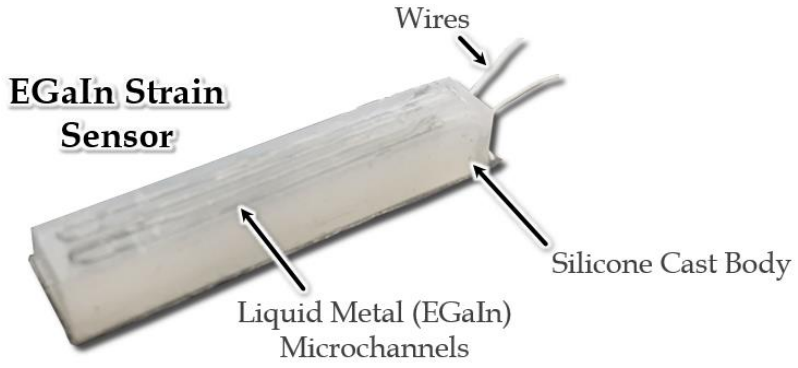

Figure 2- A soft strain sensor, fabricated with conductive fluidic micro-channels in an elastic polymer body

The body can then be treated as a variable resistor with respect to the state of its deformation. Further, the orientation and geometry of channels can be specifically chosen to optimize the sensor for a direction or pressure vs strain sensing. The concept of sensing conductive fluidic micro-channels draws from the fundamental theory of resistivity (1).

$$R = \frac{\rho L}{A} \tag{1}$$

This relationship notes that the resistance, R, of a body is dictated by its resistivity, ρ, and the ratio of length to cross-sectional area, $\frac{L}{A}$. In practical terms, as the sensor is strained in its oriented direction of measure, the increase or decrease in cross sectional area of the channels will correspond to a change in resistance across the channel ends. The mathematical realization of these changes in resistance for strain were documented in *Design and Fabrication of Soft Artificial Skin Using Embedded Microchannels and Liquid Conductors [11]*.

2.1.2 Optical Diffusion/Reflectance

Employing optical electronics as a means of sensing in soft robotic systems is a relatively new territory in the field. Various deployments of optical measurements have been investigated with substantial promise. One method involved the measurement of light diffused in a silicone body embedded with glass microspheres for increased refraction [16]. Another technique involves fabrication of an elastic polymer wave guide clad with gold foil intended to fracture and release light under loading [17]. As well, adaptions of fiber Bragg grating sensors have been deployed in soft actuated fingers [18]. The general premise behind this method of measurement is in the properties of light as it is diffused and/or reflected in silicone bodies and wave guides. For both diffusion and reflectance, there exists a source of light as well as a receiving point for the light. This can be either fibre optic or with light emitting diode (LED) packages directly embedded. These points are specifically positioned so that under the anticipated deformation, the receiver will elicit a predictable response. For the method of observing diffusion based measurements, source

and receiver are embedded within the silicone where changes in the response are the result of strain in the surrounding silicone.

2.1.3 Optical Fiducial Tracking

Typically used as a means of observing a system for testing purposes, optical fiducial tracking is a method to track the dynamic motion of soft systems. The process is fairly trivial but demands an optically sterile environment. First the soft system at hand is loaded with dark fiducials along the bending axis. A camera then observes the system, feeding the video into a computer for processing of the fiducial locations. True position along with relative motion can be deduced from analysing images over a test set [19].

2.2 Soft Actuation

Soft actuators can best be described as compliant bodies with a controllable actuation mechanism [7]. From such a broad definition we have systems that classify as soft actuators that are vastly different from one another. Shape memory alloys (SMA) have been used extensively to develop soft actuators that replicate the motion of an earthworm [20]. Pneumatic artificial muscles (PAM) have also been developed and tested as a means of imitating natural muscles [4]. The general premise behind control of soft actuators is the implementation of embedded components to specify modes of deformation desired in a body of silicone.

With actuators developed for *Programmable Soft Actuators for wearable devices* this was done with pneumatic means of actuation inside a silicone body embedded with Kevlar threading and s-glass fabric [21]. Kevlar threading served to restrict lateral expansion of

the silicone body while allowing for axial extension. The s-glass fabric was utilized as strain limiting plane in the separation of two parallel chambers. In this way, motion along a bending plane could be induced by a difference of chamber pressures while allowing stiffness to be modulated with co-inflation of the chambers. A cross sectional view of this component with embedded features can be seen in Figure 3 below.

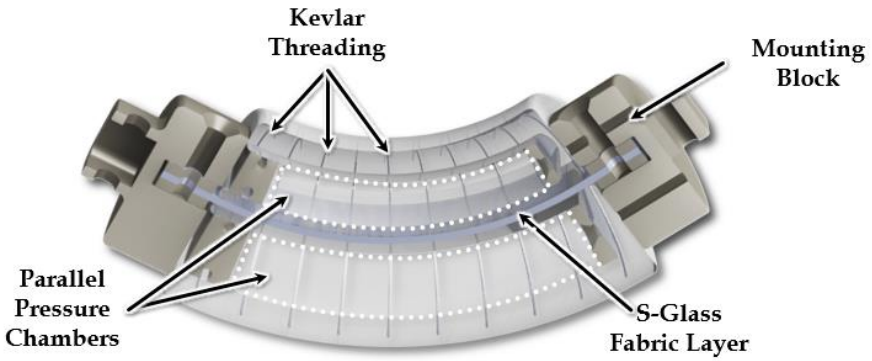

Figure 3-Cross section of dual chamber pneumatic bending actuator

2.3 Soft Robot System Modeling and Estimation

Traditional systems operate on primarily a premise of relative motion and interaction of rigid components. By contrast, soft systems operate on a foundation of stability in the deformations of a compliant structure of materials. Specifically talking about pneumatic soft actuators, this involves the coordination and fabrication of embedded materials for the desired locomotion of an actuator. These embedded components simultaneously constrain the pressurization of an actuator. From the standpoint of finite element analysis (FEA) this is a rigorous task. The complex interactions that must take

place between discreet components demands intense computation that isn't feasible for most applications. There have been successful attempts at this computation. A single chamber fiber reinforced actuator was modeled in FEA and verified under quasi-static conditions for bending in free space and in contact for force generation [2]. A bidirectional dual chamber actuator was designed with FEA for an optimal cross section in actuation of a swimming robot [3].

This process of modeling demands extensive time and modeling that is detrimental to the soft robotic design process replacing complexity with compliance. FEA creates suitable system models but at a moderate cost. An alternative option to FEA, system estimation based on observable parameters shows distinct promise for control purposes. An approach to this method is characterizing actuator position as a mapping of pressure [22]. Acquiring a coarse system model from a parameter as such may be suitable for some applications. By building on the observable parameters through embedded sensing, more robust models can be developed. A study on PAM style actuators was able to decouple system parameters of actuator length and internal pressure through EGaIn strain sensors [4]. Refining the sensing techniques and methods of analyzing the response serve to improve this method of observation.

CHAPTER 3. MEASURING MULTIMODAL DEFORMATIONS IN SOFT INFLATABLE ACTUATORS USING EMBEDDED STRAIN SENSORS

3.1 Supernumerary Grasp Assist

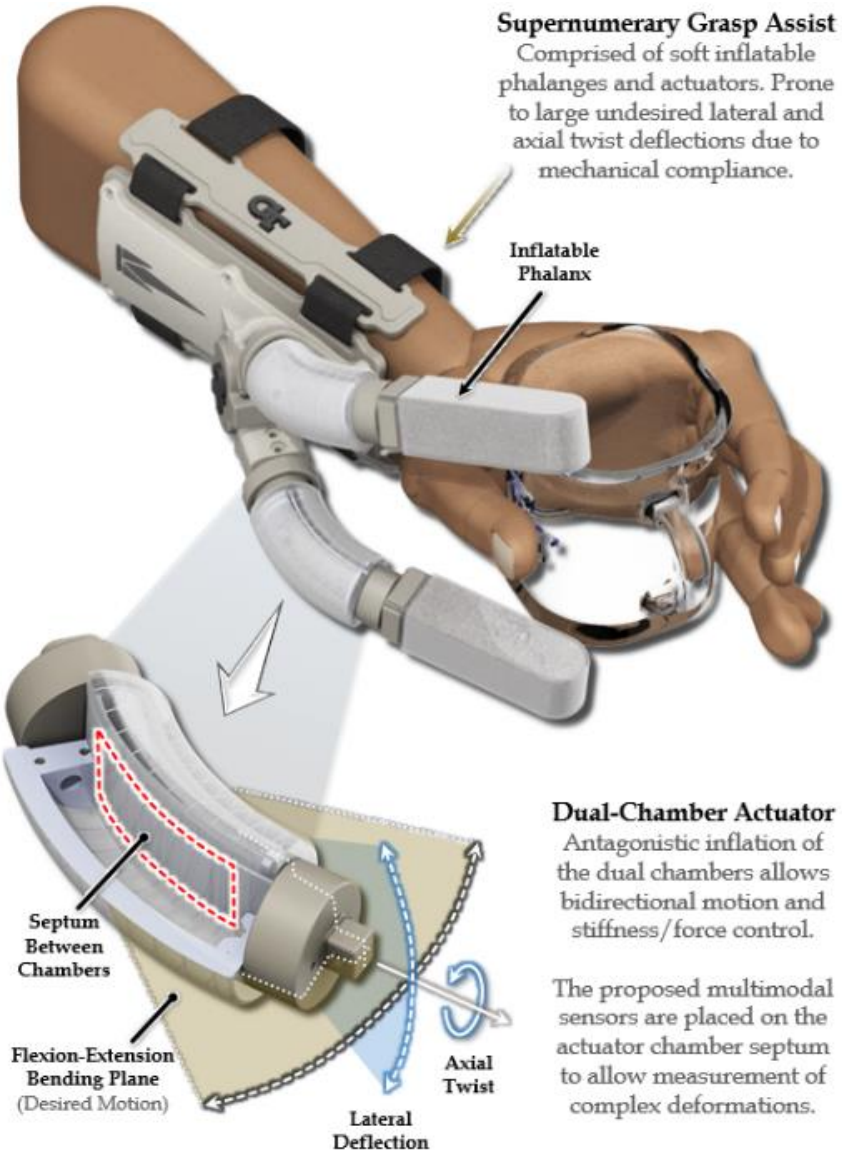

Figure 4- An illustration of the Supernumerary Grasp Assist with its inflatable bending actuator deformation modes observed when exposed to complex loading conditions in a grasp assist.

Soft robotic systems are coveted for their ability to facilitate safe, adaptive physical interactions in the presence of uncertainty. However, the same mechanical compliance that allows safety and adaptation also poses significant challenges in control. Soft robots, depending on their construction, readily undergo highly-nonlinear deformations when under complex loading conditions. These deformations are difficult to model and predict, and are even more difficult to measure and control. Inflatable actuators, in particular, are difficult to model given that the actuator bodies often undergo significant deformations in order to produce to desired motions or output forces (Figure 4). A system developed in *Variable Stiffness Pneumatic Structures for Wearable Supernumerary Robotic Devices* was designed to aid in providing grasp forces to a user suffering from dexterous hand impairment as the result of a stroke [23]. The system, seen in Figure 4, is composed of dual chamber soft bending actuators and variable stiffness inflatable phalanx as the digits to assist in grasping.

One method of controlling soft inflatable actuator position is to infer the actuator position from a mechanical model and its measured internal pressures. Recent work in soft actuator modeling demonstrated that accurate analytical models can be used to accurately predict inflatable actuator deflection under specific environmental conditions and internal pressures [22, 24, 25]. While such methods are effective when loading conditions are well-defined, these models cannot accommodate complex, variable loading conditions which could heavily influence actuator mechanics, and do not include sensors which could enable closed-loop control. In addition, the use of compressible, fluid media which undergo density changes due to ambient pressure and temperature affects the accuracy of model predictions.

An alternative to analytical model-based, open-loop control of inflatable soft actuators is the use of embedded sensors which provide feedback on their current deformation modes. Recent research along these lines involved using embedded carbon nanotubes [26] and conductive liquid channels to measure bulk bending actuator strains [15, 27, 28]. Other work utilized soft sensors strategically placed at bending-induced stress concentrations to measure soft body deflections [14]. Optical waveguides and diffusion-based approaches which measure optical scattering and attenuation as a means of inferring relative shape change have also gained traction as solutions of measurement of complex motions in soft devices [17, 29, 30]. Thus far, these techniques have been used primarily to measure single degrees of deformation, but are not extended for the multimodal deformations seen in practical applications.

In this paper, we embed conductive-liquid based soft strain sensors in pneumatic bending actuators to measure multiple modes of deformation. These actuators, when implemented in supernumerary grasp assist devices to enable flexion and extension of robotic fingers (Figure 4), often undergo lateral deflections and twisting due to contact with objects [31]. These typical but undesired deformations must be measured to accurately control grasp postures. Here, we develop soft sensors to capture both the primary (i.e. desired) deformation of the actuators and lateral and twisting deflections seen during actuator use, and we evaluate their performance on benchtop and application tasks.

Section 3.2 discusses the design rationale used for the soft sensors and how sensors are placed to measure multiple deformations. Section 3.3 describes the fabrication of the sensors. Sections 3.4 details the results of experiments conducted to evaluate multi-modal sensor performance both independently and within pneumatic bending actuators, and the

efficacy of sensor-embedded bending actuators when utilized for proprioceptive feedback in grasp assist devices. Sections 3.5 discussed insights gleaned from this work and future research directions based upon these findings.

3.2 Sensor Placement for Multimodal Deformation

This work is inspired by the authors' previous research [21] involving variable stiffness inflatable components for grasp assist devices. Central to this work was the design of a dual-chamber, bidirectional bending actuator. Though this soft actuator was meant to provide flexion-extension motions, it was prone lateral deflections and axial twists depicted in Figure 4. To detect and correct for off-axis deflections, we employ embedded sensors which can undergo the same deformations and therefore allow tracking of them.

3.2.1 Differential Strain Measurement

Given that the actuator is intended for bending motion, the most natural location for strain sensors used to measure the bending angle is at the planar actuator septum. Here, the midline is constrained in extension by an inextensible fabric layer, but elastic material placed on either side of the septum with undergo tensile (convex) or compressive (concave) strains, depending in the direction of curvature (Fig. 5). Applying soft strain sensors on both sides of the septum-oriented in the direction of maximum strain - allows the measurement of differential strain. Measuring strain on both sides of the septum, rather than just one, provides more reliable data and makes determination of bending direction easier. Using (2) and (3), and assuming pure bending of the septum, the flexion bending angle θ and direction can be calculated from the estimated arc lengths s_1 and s_2.

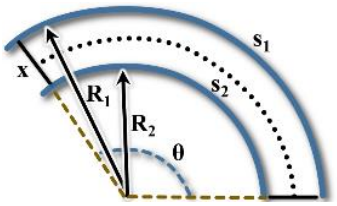

x = distance between microchannel layers, known
s_1, s_2 = arc lengths from sensor output, measured
R_1, R_2 = respective radii sensors make, unknown
θ = ultimate angle that the arcs form, unknown

Fig. 5. Pure bending model of an elastic strip with an inextensible septum

$$s_1 = R_1 * \theta; s_2 = R_2 * \theta; \quad (2)$$

$$R_1 = R_2 + x; \ \theta = \frac{s_1 - s_2}{x} \quad (3)$$

3.2.2 Measuring Lateral and Twist Deformations

This sensor placement rationale is well-suited to the measurement of pure bending, but does not support sensitivity to lateral deflection and twisting, as evidenced by data in Figure 6. To accommodate these deformation modes, we consider the geometric effects of those modes of strain on the actuator septum. For lateral deflection, we assume that the transverse midline of the septum will undergo no tensile or compressive strain, while areas on either side will undergo strain depending on distance from the midline - similar to the bending strain case. By placing sensors away from the transverse midline, we improve sensitivity to pure lateral bending. For differential measurements, sensors are on opposite sides of the midline.

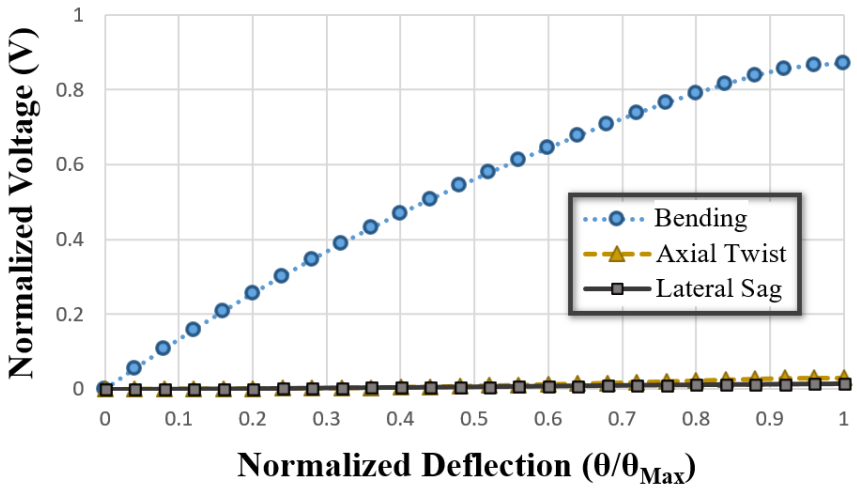

Figure 6- Data illustrating the insensitivity of the axially-aligned, opposing pair sensors to twist and lateral deformations.

To measure axial twist, we again consider the strains in the septum during the deformation mode. Similar to other deformation modes, the central axis of the septum undergoes not change in length, while any lines parallel but offset from the central axis experience a change in length. Lines oriented at diagonals would undergo even more strain than lines parallel on the central axis. Aligning a sensor pair diagonal to the central axis and parallel to each other would then allow differential measurement of actuator twist angle.

3.2.3 Increasing Sensitivity to Deformations

The degree of strain in a region of body due to bending or twist is proportional to the distance of the strain region from the central plane or axis of deformation. This rationale dictates that the soft sensor pair should be located near or on the outside of the pneumatic bending actuator body, given that strain will be the largest there during any deformation mode. However, the actuator body undergoes large, inconsistent strains at it outer layer during inflation, which would distort sensor output and affect reliability of readings. In

addition, the outer layer of the actuator will occasionally make contact with external bodies, exposing the soft sensors to normal or shear forces which change the strain state. To reduce susceptibility to external contact while increasing sensor sensitivity, the soft sensor pair is mounted soft ridges - which are attached to the septum - so that their distance from the septum midline is increased (Figure 7).

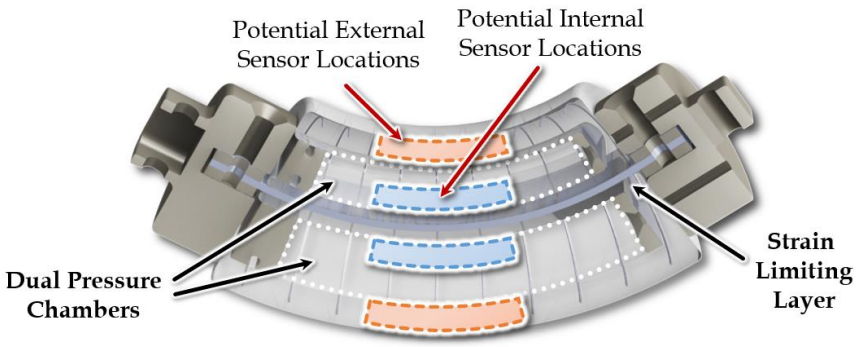

Figure 7- Proposed sensors embedded directly on the strain limiting layer

The final multimodal soft sensor design is shown in Figure 8. The soft sensor pair is comprised of a silicone rubber substrate with eutectic Gallium Indium (EGaIn) filled serpentine microchannels aligned with the direction of strain to increase sensitivity. The sensors are offset from the strain limiting layer with a 4.0 mm silicone ridge. The fabrication process for the sensor pair is described below.

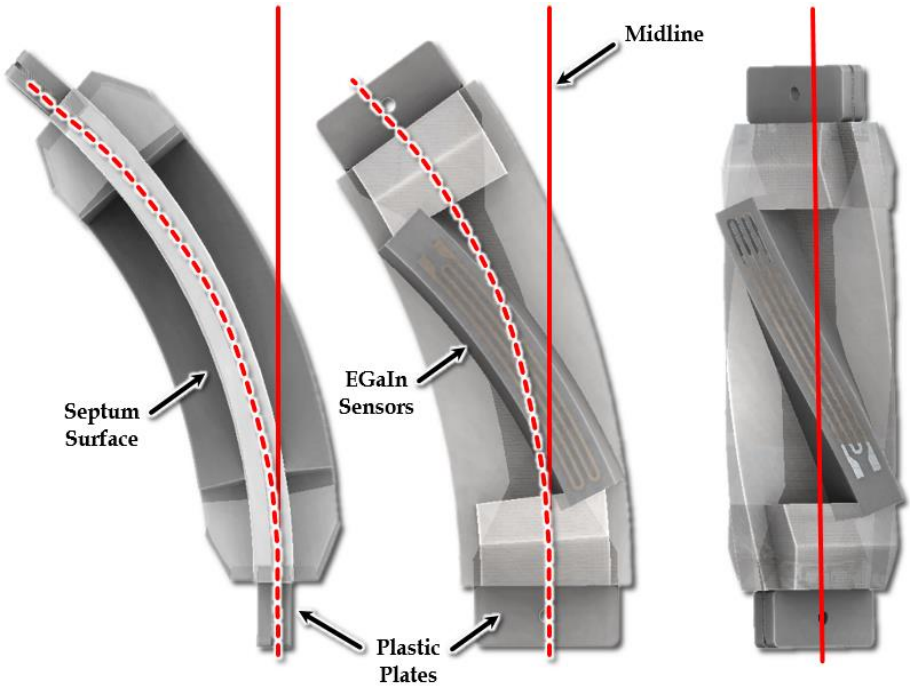

Figure 8- Illustrations of the pure modes of actuator septum deformation: bending (left), lateral deflection (middle), and axial twisting (right).

3.2.4 Sensor-Embedded Actuator Design

The proposed multimodal bend sensors are designed to be embedded within a pneumatic bending actuator. The embedded sensor design used in this work is based on the dual-chamber pneumatic actuators designed for grasp assist devices [23]. For these actuators, the sensorized strain limiting layer (septum) is fabricated independently and installed in an actuator body. This modularity allows the experimental evaluation and redesign of the sensors without complicating the entire fabrication method.

3.3 Fabrication of Sensor Embedded Actuators

The ridge-mounted sensor pair and the actuator septum body were fabricated separately before being combined as the final step of the manufacturing process (Figure 9).

3.3.1 Test Septum Fabrication

The ridge-mounted sensor was manufactured in three fabrication steps. The molds for the sensors and septum were printed on an Objet30 Prime (Stratasys, Ltd.) polyjet 3D printer, while all embedded plastic pieces were printed on a Fablicator 3-D Printer (K&L Services Group, Inc.).

- Step 1: Braided copper wire (36 AWG) was fed through holes in the sensor mold. Silicone (Dragon Skin 10 Slow, Smooth-On, Inc.) was poured into the molds and a flat, acrylic cover was placed on top to seal them. Each casting produced silicone bodies for two sensors.

- Step 2: After curing, sensor halves were adhered together using silicone adhesive (Sil-Poxy, Smooth-On, Inc.). A hypodermic needle and syringe were used to inject eutectic Gallium-Indium (EGaIn), filling the channel and creating a connection between the wires.

- Step 3: The resulting sensor was placed into the bottom of ridge sensor mold (Figure 9), which was then filled with silicone (EcoFlex 30, Smooth-On, Inc.) and capped with an acrylic lid. EcoFlex 30 was chosen due to its lower Shore hardness which minimizes the effects of the ridge on septum on resistance to deformation.

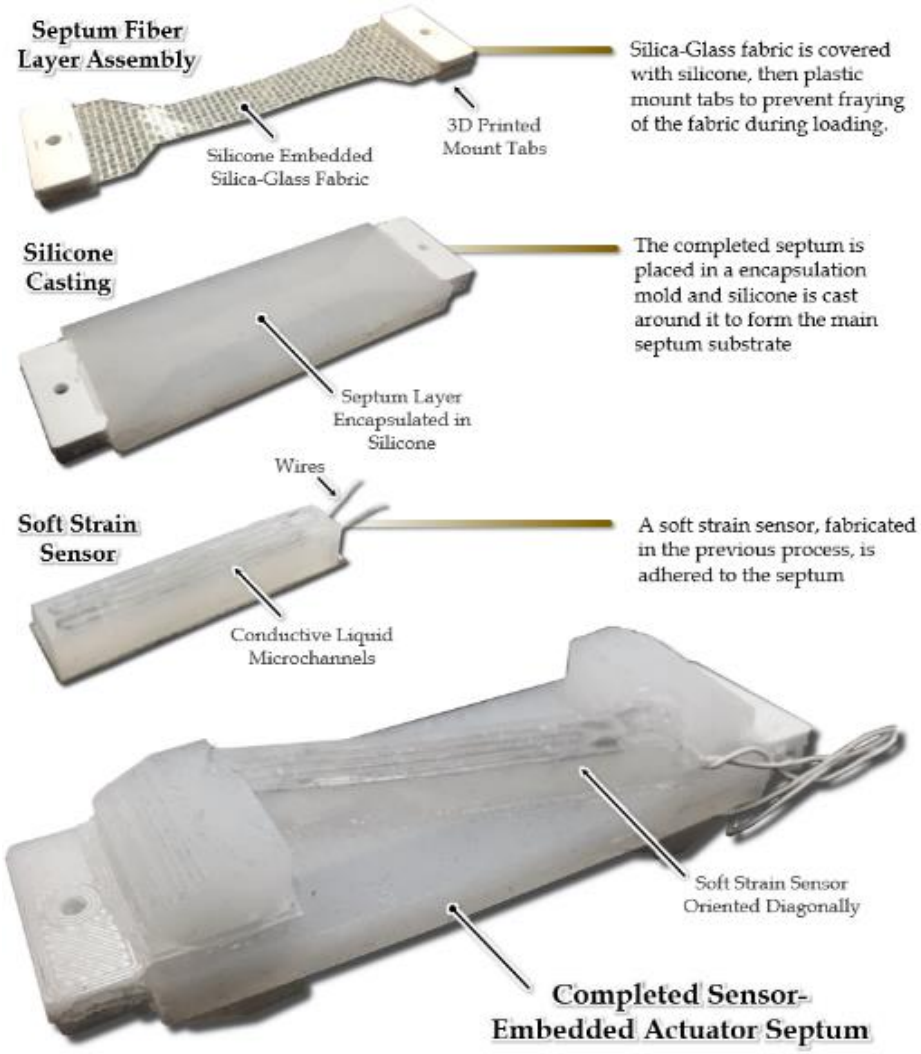

Figure 9- Fabrication steps for the sensorized actuator septum which allow measurement of multiple modes of actuator deformation

The test septum body was constructed using two main steps:

- Step 1: A strain-limiting layer was made from silicone encapsulated fiberglass, which was cut into an hourglass shape on a laser engraver (Universal Laser Systems Inc.). Four plastic plates were then attached with silicone adhesive, two at each end (Figure 9).

- Step 2: The strain-limiting layer was inserted into a 2-part mold and fixed with pins through the PLA plates to prevent movement during casting. Silicone was injected via syringe into the ports on the top of the mold.

Completed ridge-mounted sensors (Figure 9) were then attached to the septum body with Sil-Poxy, such that opposite corners of the sensor were coincident with the edges of the septum. Sensors were attached to both sides of the septum so that they mirrored each other. Finally, four silicone blocks (Dragon Skin 10 Slow) were attached via Sil-Poxy in the areas between the sensor and the PLA plates to further simulate conditions of an embedded sensor.

The overall length of the test septum was 82 mm, with a deformable length of 65 mm. Sensors were arranged such that they were roughly 19.6 degrees offset from the central axis, with a ridge height of 4mm. Once completed, the sensorized septum is embedded in an inflatable bending actuator using a process similar to in [23](Figure 10).

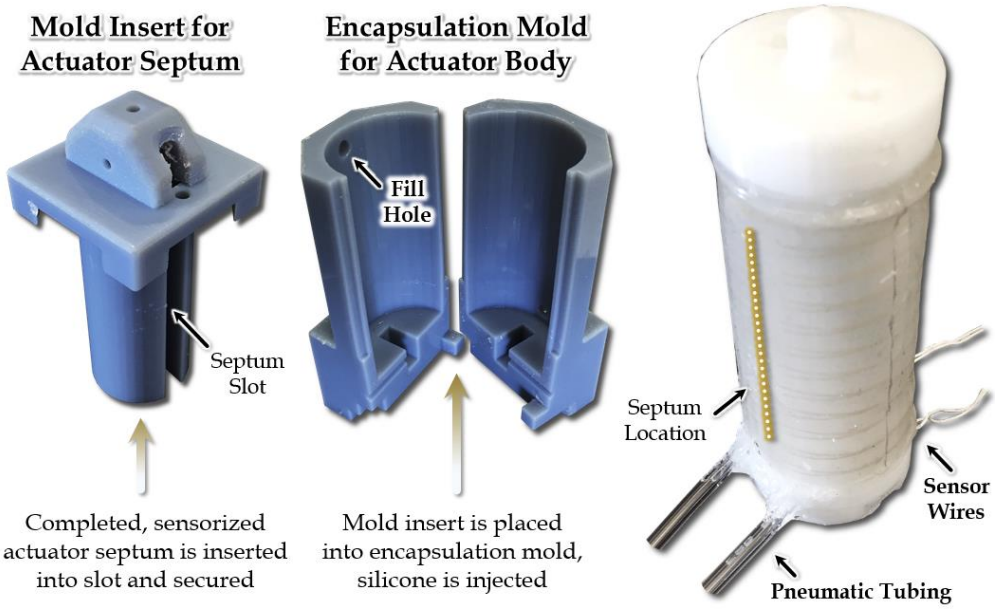

Figure 10- Photos of the pneumatic bending actuator assembly process, with the completed bending actuator shown on the far right

3.4 Characterizing the Test Septum

3.4.1 Pure Bending

In order to measure sensor responses to pure bending, the septum was loaded axially on the Instron and pinned at each end to allow rotation at the joints (Figure 11). Starting with the test septum fully extended, the top crosshead was lowered 30 mm in order to induce a bend and then immediately brought back to the zero position while recording voltage response on the National Instruments myDAQ device.

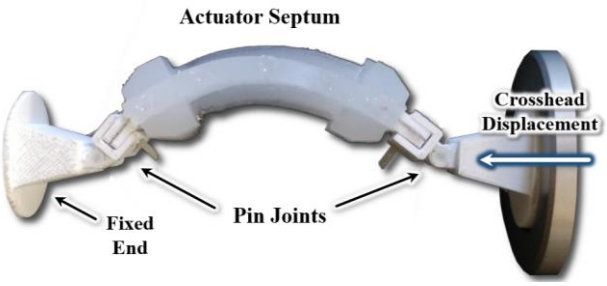

Figure 11- Photo of the experimental setup (oriented at 90°) to characterize the response of the sensorized septum to bending deformation.

Bending tests can be seen in Figure 12 and Figure 13. The polynomial fit line shows an approximate maximum change in voltage of 0.13 V for sensor extension and a -0.08 V change for sensor compression. More hysteresis was seen when the sample was cycled at higher rates, with the best fit line returning to a point approximately 0.2 V away from the starting point in the 2.5 second cycle run.

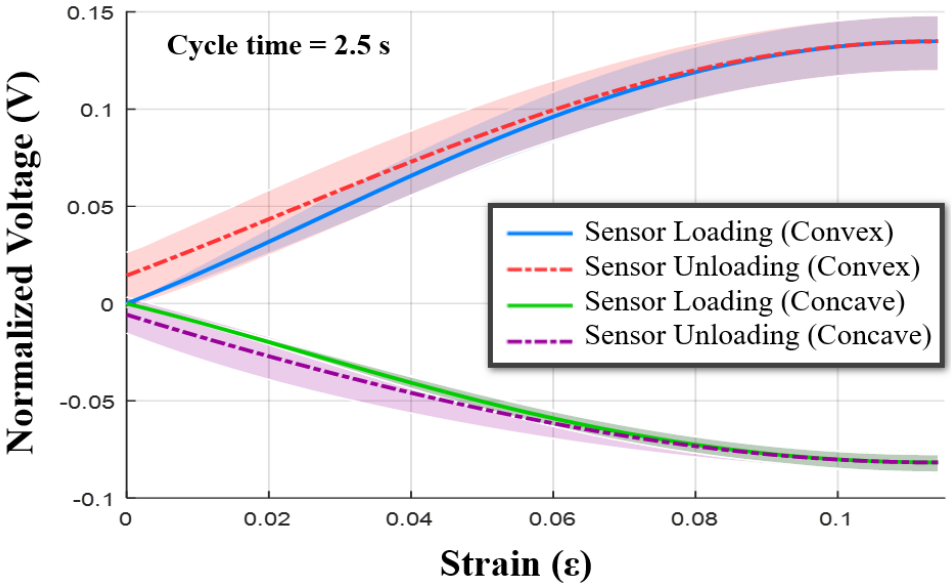

Figure 12- Response of the strain sensor pair as the actuator septum undergoes pure bending at 2.5-second cycle times. Hysteresis was greater for faster cycle times, as the sensor has less time to relax and return to its idle state.

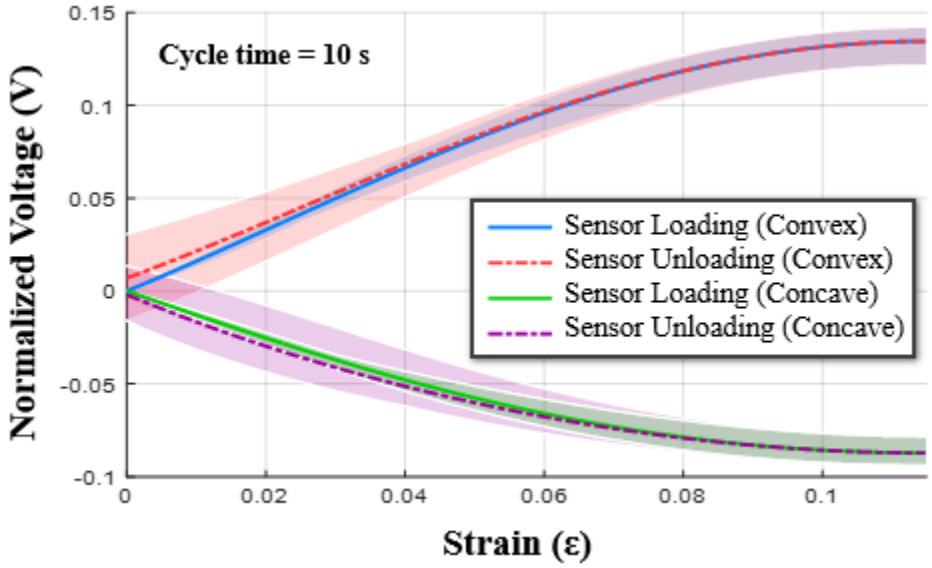

Figure 13- Response of the strain sensor pair as the actuator septum undergoes pure bending at 10-second cycle times. The sensor responses are less hysteric but have larger variances when under less strain.

3.4.2 Pure Twisting Experiments

In order to convert the linear motion of the crosshead movement into rotational motion, a testbed was designed and printed on a Fablicator 3D printer (Figure 14). The test septum was held stationary at one end while the other was fixed to an axle which could rotate radially to the septum. The axle contained two pulleys; one which had a Kevlar cable that ran to the upper, mobile crosshead of the Instron, and the other which ran a cable to a pre-tensioned elastic band. By running wrapping these pulleys in opposite directions, the elastic band provided a counter-force to the crosshead movement, allowing the test septum to return to its original position in the unloading stage. As the pulley connected to the Instron crosshead was 27.5 mm in diameter, the Instron crosshead was raised 21.5 mm to achieve a 90-degree rotation.

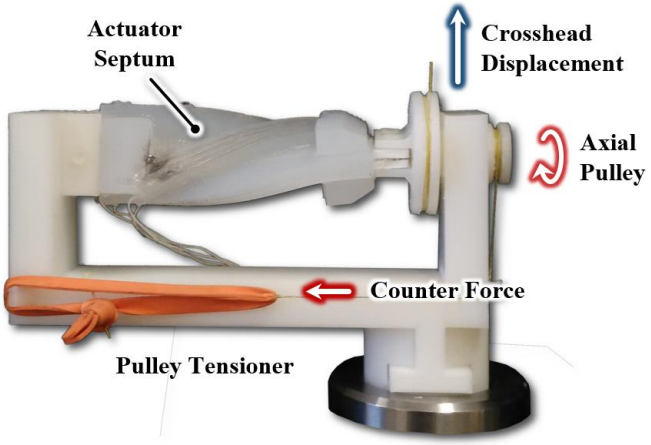

Figure 14- Photo of the experimental setup for axial twist sensor characterization, where the tester crosshead drives an axial pulley via cable.

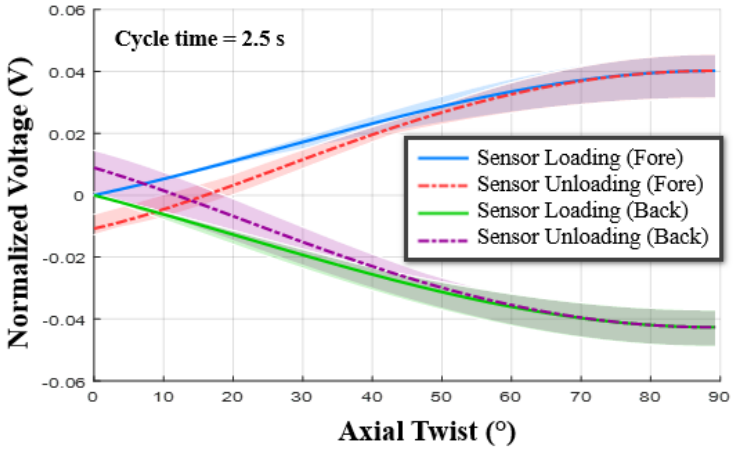

Figure 15 -Response of the strain sensor pair as the actuator septum undergoes axial twist deformations at 2.5-second cycle times. Hysteresis is greater here than that seen in the 10-second cycle time (not shown here).

Figure 15 depicts results from the twist tests. The maximum value for the sensors in extension and compression were approximately 0.045 V and -0.04 V, respectively. As with bending, notable hysteresis is seen at faster cycle speeds.

3.4.3 Pure Lateral Deflection

Lateral deflection in the test septum was tested using the testbed seen in Figure 16. One end of the test septum was held stationary while the free-end was cantilevered out beneath the Instron load cell. A Kevlar thread was run from the upper crosshead to the free end of the septum, allowing it to be deformed upwards as the upper crosshead was raised. To prevent twisting or buckling, guardrails were added on either side of the free-end to constrain lateral motion. Tests were run over a range of 15 mm.

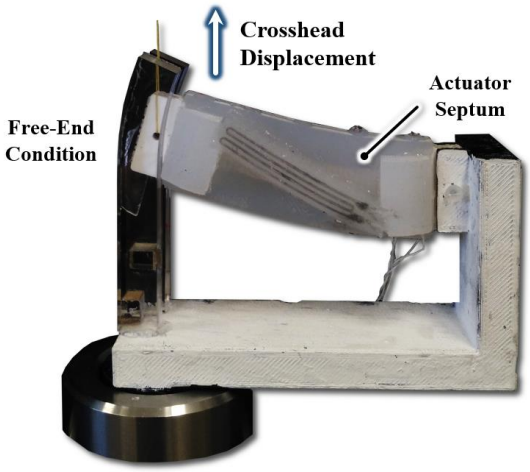

Figure 16- Photo of the experimental setup for lateral deflection sensor characterization, where the tester crosshead drive loads the septum via cable.

Results from the deflection test are shown in Figure 17. Only one sensor is shown as the data from the opposing sensor displayed too much noise to apply a polynomial fitting. The maximum voltage reading for the curve fit was approximately 0.017 V, a magnitude less than twist and bend readings.

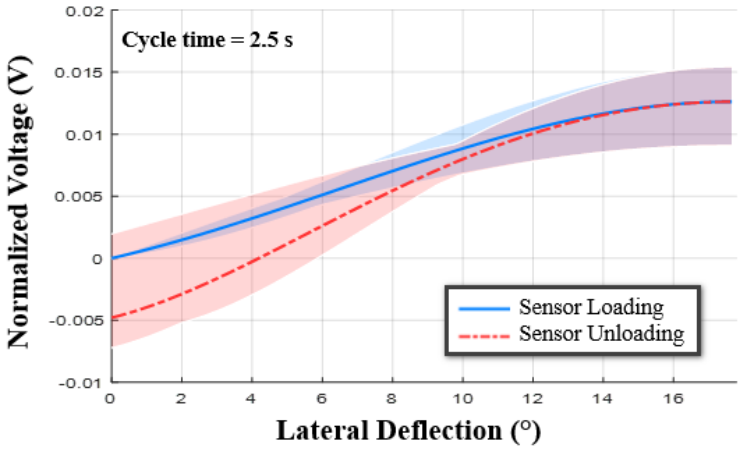

Figure 17- Response of the strain sensor pair as the actuator septum undergoes lateral deflection at 2.5-second cycle times.'

3.5 Embedded Sensing Baseline

Next, the calibration data taken in the previous section was used as a basis for bending actuator state estimation. Three pure modes of deformation were tested and the output and calibration data are compared. Ground truth for actuator deformation was measured using an electromagnetic tracking system (trakSTAR, Ascension, Inc.).

3.5.1 Actuator Bending

To collect bending data, the actuator was mounted to a table and positioned such that the sensor faces were parallel to the floor (Figure 18). Two forms of bending were investigated in this test: bending due to pressurization and bending due to unpressurized loading.

For pressure-induced deformations, the bottom chamber was inflated so that the actuator bent upwards. Pressurization was done stepwise and voltage readings were recorded at each step, ranging from 0-8 psi in 1.0 psi increments. For force-induced

deformations, weights were suspended from the cantilevered end of the actuator in steps of 100 g.

Results from testing (Figure 19) show that sensor outputs loosely follow the expected response to bending for the vented actuator, but that they deviate significantly from the expected response when the actuator is pressurized.

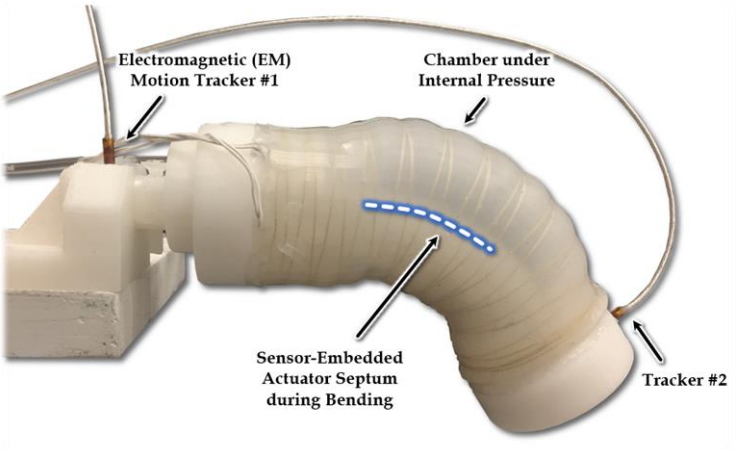

Figure 18- The sensor-embedded bending actuator inflated for flexion motion. Electromagnetic trackers served as ground truth for angle measurements.

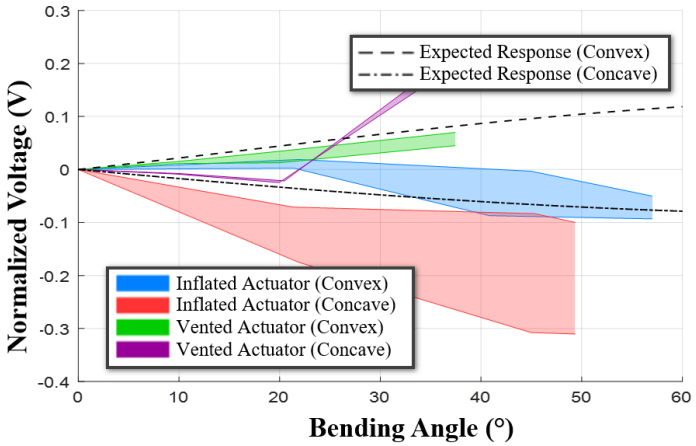

Figure 19- Response of the sensors to actuator bending under internal pressure and in a vented state. Internal pressure clearly affects sensor output.

3.5.2 Actuator Axial Twist

Twist data was recorded by inserting an acrylic plate beneath the actuator to prevent deflection or bending. A hanging basket was hung from a lever arm attached to the far end of the actuator. Weights were placed in this basket to induce a rotation, starting at 0 g progressing to 400 g in steps of 100 g. The lever arm length was 25 mm from the neutral axis of the actuator. Figure 20 displays the behavior of the sensors observed during this test.

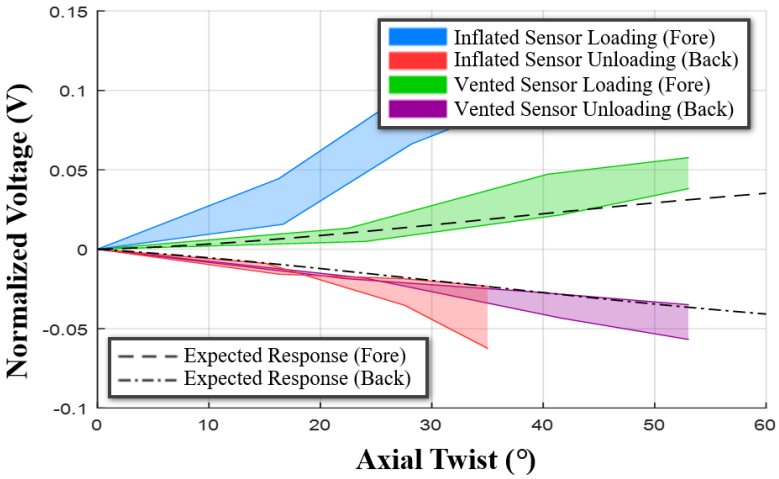

Figure 20- The responses of the embedded sensor pair as both inflated and vented pneumatic actuators underwent axial twist deformations.

3.5.3 Actuator Lateral Deflection

To measure deflection, the actuator was loaded into the table mount at a 90-degree angle, such that the septum was perpendicular to the ground. The actuator was loaded by hanging weights from its distal end. The amount of weight progressed through 0, 75, 150, and 225 grams. Results of this test, seen in Figure 21, show that the soft sensor outputs resemble the expected, sigmoidal shape as deflection increased. Results also show that the

sensor readings varied widely and that one sensor was more responsive than the other (should be similar, if not identical).

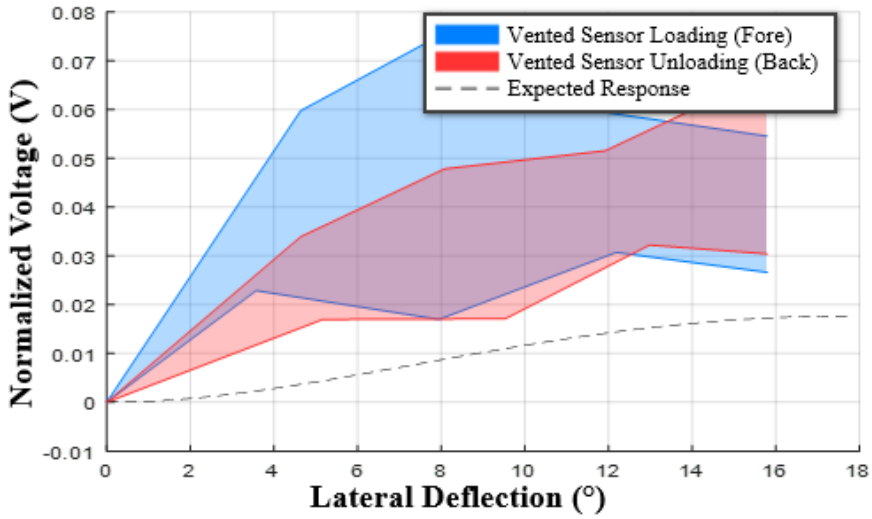

Figure 21- Plot of sensor responses to lateral actuator deflection.

3.5.4 Investigating Pitfalls

The behaviour exhibited by sensors in the pressurized actuator did not follow the predicted models from testing the independent septum. Although some deviation was anticipated from the ideal conditions, the results from actuator testing proved further investigation was necessary to determine what caused the substantial deviation and what could be done to alleviate it. Figure 22 shows a short investigation of the internal deformations present in the actuator. An actuator was fabricated with SortaClear 18, a translucent silicone with comparable mechanical properties to DragonSkin 10. The SL layer of this actuator was marker with a red grid so that the mechanical behaviour of the septum could be seen. From this test, it was concluded that primary bending yielded a lateral concave bowing along with primary bending under pressurization.

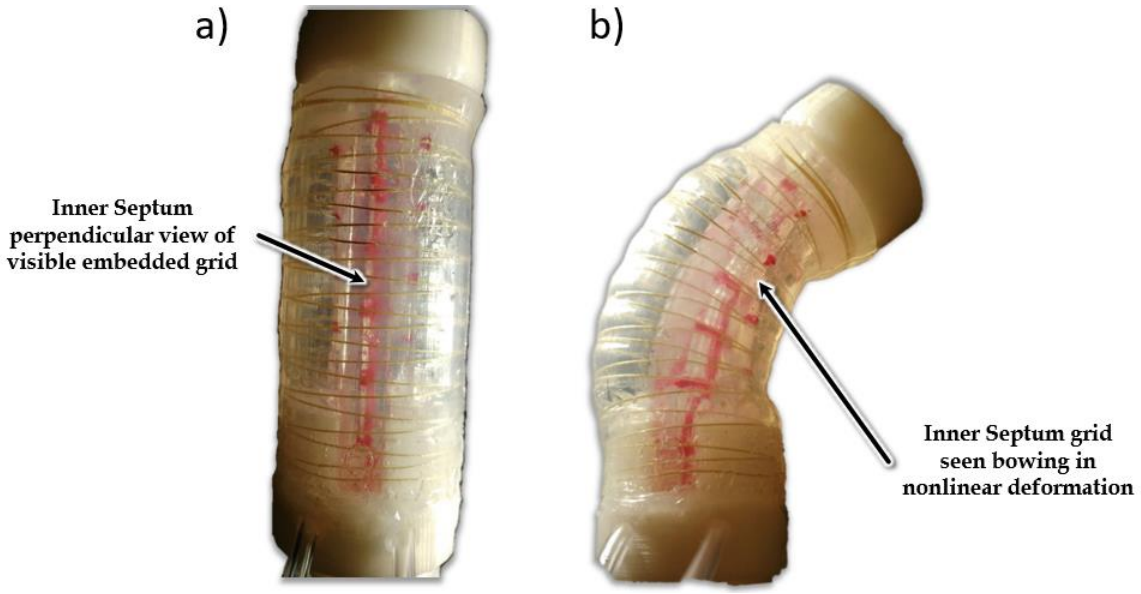

Figure 22- Actuator fabricated from transparent silicone with a visible red grid imprinted on the septum for qualitative optical analysis in (a) vented and (b) pressurized states.

3.6 Practical Embedded Sensing

Multimodal sensor-embedded actuators were installed in a supernumerary grasp assist device to determine their ability to generate proprioceptive feedback for human users under realistic usage conditions (Figure 23). Voltage responses from the sensors was acquired using a microcontroller (Arduino, Inc.), and converted to pulse width modulated signals to control vibro-tactile motors. Motors were sewn into two nylon arm bands, one worn at the wrist and another near the elbow, to provide feedback to human subjects. A datum for each sensor was taken from the average voltage readings over 10 seconds as the system was idle. The datums were set to correspond with a midpoint intensity on the vibrating motors. Changes in sensor voltage output were conveyed to subjects as proportional changes in vibration intensity in the corresponding motors.

3.6.1 Proprioception of Actuator Deformation Degree

Tests were performed to establish whether a human subject could sense the extent of actuator deformation based on vibro-tactile feedback. In these tests, only sensitivity to deformation degree was under scrutiny, so subjects were made aware of the mode being tested. Each experiment consisted of three trial types: bend, twist, and deflection.

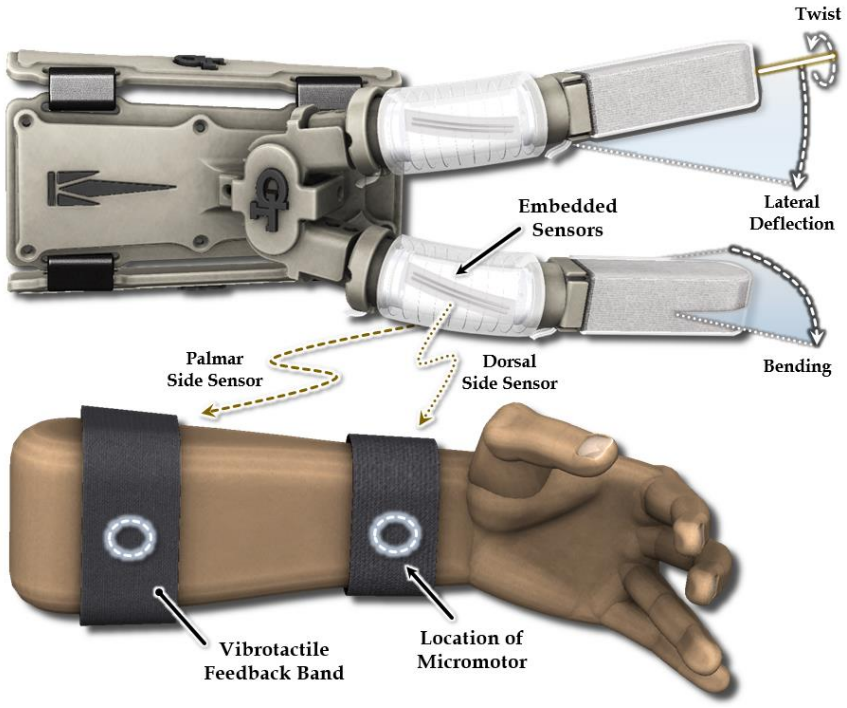

Figure 23- Supernumerary grasp assist device set up for actuator deformation experiments; the multimodal sensors provide proprioceptive feedback.

Before testing, the subjects donned the vibrotactile feedback bands and were allowed to handle the sensor-embedded septum to familiarize themselves with feedback for five minutes. The subject was then positioned such the test setup or experimenter were not visible. Finally, the subject was told which form of deformation would be tested.

The experiments consisted of three possible configurations: zero position, median, and max deformation. In bending and twist, the midway point and maximum deformations were 45

and 90 degrees, respectively. For lateral deflection, they were 8.0mm and 15.0mm. Nine trials were run, each with three iterations of each configuration of the septum, arranged in randomized order. Trials consisted of deforming the septum, recording the subject's response, and then returning to the zero position. The subject was told when the septum was returned to the zero position and asked to respond once the septum was in the desired state.

Table 1 shows that feedback from the multimodal sensors allowed subjects to determine coarse degrees of deformation. Bending angles were correctly identified 83.3% of the time, while 16.7% of incorrect answers were one angle step off. Guesses for lateral deflection and axial twist were less accurate, both at 66.7% correct.

Table 1- Proprioception of Actuator Deformation Mode and Degree

	Deformation Mode Guess				*Bending Angle Guess*		
Mode	***Bend***	***Twist***	***Lat.***	*Angle*	***0º***	***45º***	***90º***
Bend	5	1	0	***0º***	5	1	0
Twist	1	4	1	***45º***	1	4	1
Lat.	0	0	6	***90º***	0	0	6

The left half of the table contains data on human proprioception of bending angle, enabled by the developed sensor-embedded actuators. The right half of this table contains data on proprioception of deformation mode.

3.6.2 Determination of Form of Deformation

The next experiment tested human ability to discriminate between different modes of actuator deformation using multimodal sensor feedback. During each of nine trials, the actuator septum was deformed in a specific mode and the subject asked which form of

deformation it was undergoing. Each mode appeared three times in random order. For this experiment, one of two possible directions for deformation was chosen for each mode to simplify the test condition.

Data shown Table I indicate that multimodal sensor-driven vibro-tactile feedback is effective in enabling discrimination of deformation modes, though this experiment was only moderately challenging for the subjects and did not involve directionality and degree of deformation.

3.7 Discussion

3.7.1 Independent Sensor Performance

Tests of the sensor-embedded actuator demonstrated that multiple soft actuator deformation modes can be measured with a simple embedded structure. The accuracy and precision of the deformation measurements was limited due primarily to electrical noise, oxidation of the conductive liquid and mechanical artifacts as conductive liquid and wires moved inside the silicone bodies, but the range of sensor outputs for each deformation mode remained stable after multiple trials. Electromagnetic and mechanical interference can be addressed using improved amplification techniques and more secure sensor wire attachment points.

3.7.2 Effectiveness of Sensors Embedded in the Actuators

Once embedded in the pneumatic bending actuator, the soft strain sensor responses to each deformation mode deviated significantly from expected performance, which was based on the independent sensor characterization experiments. Though voltage outputs

from the sensors loosely followed the expected behaviors, structural changes such as the septum bowing likely distorted the deformation pattern throughout the sensor body. Ambient pressure changes were not shown to significantly affect the independent soft sensor output in separate pressure test (results not shown here), but the internal pressures of the actuator likely change deformation mechanics in different modes due to compression of the fluid media, and small, unexpected deformations – such as wall buckling and septum folding - in critical regions of the device.

Despite significant electromechanical noise and distortion observed in multimodal sensor outputs, human subjects were able to use the feedback for discrimination of deformation modes and coarse changes in degree of deformation.

3.7.3 Implications for Real-World Applications

The accuracy issues observed when using multimodal sensors to measure pneumatic bending actuator deformations highlight needs for improvements in implementation, but the feasibility of using such sensors in real-world applications remains promising. Implementation can be improved by:

1. Employing a more robust sensor type (e.g. soft optical sensors) as conductive liquid based sensors can be highly susceptible to mechanical failures and electrical noise
2. Distributing more sensors in the soft device of interest to capture subtle the deformations which could markedly improve estimates of soft device shape, and
3. Optimizing sensor placement such that deformation predictions for be maximized for a given sensor suite.

Investigation of these improvements to implementation and feasibility is made more tractable by the low-cost of designing and fabricating elastomer-based soft sensors.

3.8 Conclusion

This paper presents a method for tracking the deformation modes of soft inflatable bending actuators used in grasp assist devices. Soft strain sensors were designed and strategically placed within an inflatable bending actuator to allow measurement three distinct deformation modes: bending (primary, desired deformation mode), lateral deflection, and axial twist. Results demonstrates that the multimodal sensors enable discrimination of deformation mode and degree, but that precision and reliability of the sensors - once embedded in an inflatable device - can be comprised by the complex, nonlinear deformations of the device itself. The multimodal sensors, despite not showing high efficacy only in actuator experiments, still enabled proprioception in soft human augmentation devices.

CHAPTER 4. **ASSISTIVE GRASP APPENDAGE (AGA)**

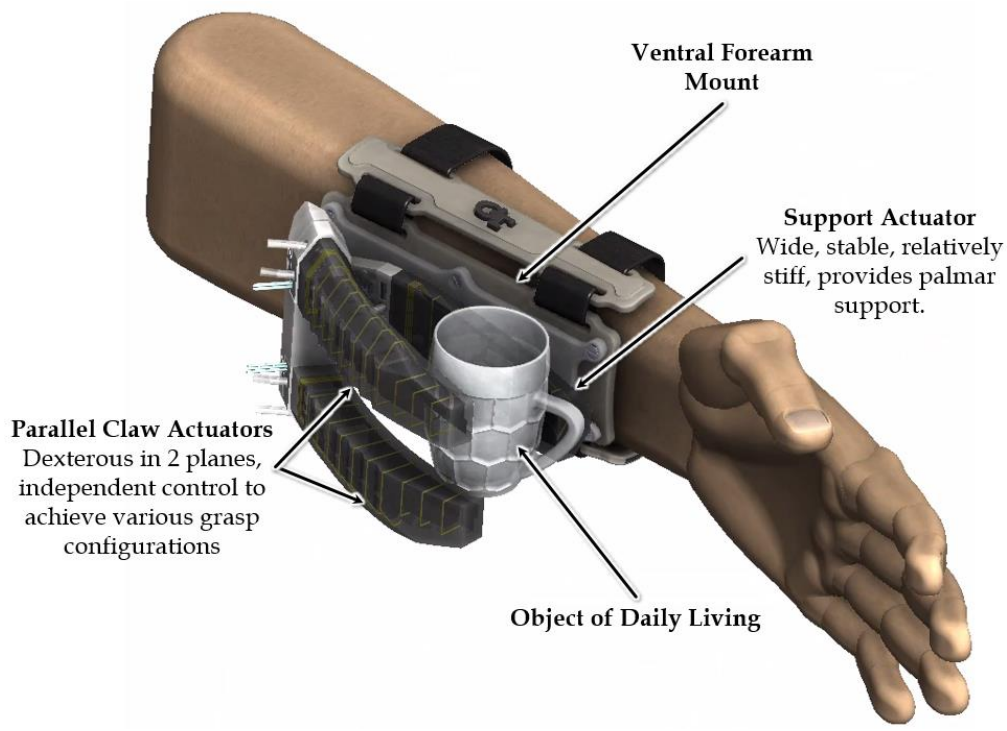

Figure 24- Rendering of AGA in grasp of an object with primary chambers inflated to match the curvature

Control of soft robotic systems is not as intuitive as its traditional counterpart. The same mechanical compliance that yields their ergonomic and economic benefits renders them difficult to model. This chapter presents a novel method of soft sensing for the positional characterization of soft actuators as feedback control of a complex system of sensors and actuators. An actuator designed for dynamic motion in perpendicular directions was outfitted with fiber optic components responsible for observation of the silicone body under multimodal deformation. Response from the embedded sensing was then used to train a linear regression to characterize position of the actuator tip 1mm accuracy. This sensorized actuator was mirrored laterally and positioned opposing a palmar actuator capable of determining grasp quality through embedded force sensing resistors (FSR). With this complete grasping assembly mounted on a wrist bracket and coupled

with EMG inputs from a user, it could be utilized as a soft, lightweight, robotic orthotic hand. This hand was capable of adaptively grasping various objects commonly associated with everyday living with varying forms and textures.

4.1 INTRODUCTION

A technology is valued primarily by its most capable application. The past two decades have been spent developing and benchmarking the field of effective soft robotic techniques. Expanding the field demands research and development of complex actuator systems with integrated sensing for their use in practical applications. In designing complex practical systems the priorities of fundamental research can be established.

A substantial benefit of soft robotic systems is in their freedom of form factor. The physical shape of the inflatable vessel can be comprised of whatever geometry facilitates the desired motion of the system. This freedom allows a designer to incorporate grasping solutions that sacrifice complexity and precision with compliance. This quality comes at the cost of control. Soft systems often cannot be modeled intuitively by free body or bending diagrams for estimating response. The elasticity of the body is akin to innumerable degrees of freedom that becomes increasingly complex with the various embedded shape constraining components. Taking the road of finite element analysis is incredibly demanding for similar reasons, and has only been successfully validated in a few instances [2, 3]. This leaves the most appealing method of control to be through sensory feedback. A number of investigations show promise for this approach. In the authors' previous work pneumatic actuators were embedded with EGaIn strain sensors to decouple modes of

deformation from chamber pressure[9]. A full grasp mechanism was fabricated monolithically with sensors embedded for feedback.

The system to be discussed is a novel design for a device that may be used as an additional grasping point for a fully capable user or an independent grasp mechanism for a user who has limited or no control of their hand. The overall intent of the system is to provide a grasping solution capable of fulfilling the majority of a user's grasping needs at low system cost and complexity by using soft actuators. Traditional myoelectric prosthetics are relatively expensive while providing marginal capabilities of a standard hand. This is due to the level of complexity required to operate grasp mechanisms of complex independent digits. Further, controlling these digits to operate intuitively likely impedes fine control that could fully utilize the precision. By designing prosthetics from a foundation of soft robotics, compliance and adaptive materials can replace the precision of traditional robotics.

4.2 Sensorized Actuator Design

The outlined grasping prosthetic serves as a vehicle to demonstrate the capability of deformable reflective diaphragm sensors embedded in soft pneumatic actuators. To test the full capability of the sensing method, actuators were designed capable of controlled bending in two independent directions. The actuator design was further equipped with fiber optic cables, diodes required for emitting and receiving IR light, and a reflective diaphragm molded internal to the primary chamber. Deliberate arrangement of the optical components enabled partially independent response of the three photodiodes to the desired modes of

actuation. The response coordinated with ground truth measurement of position was used to train a linear regression to estimate position of the actuator tip.

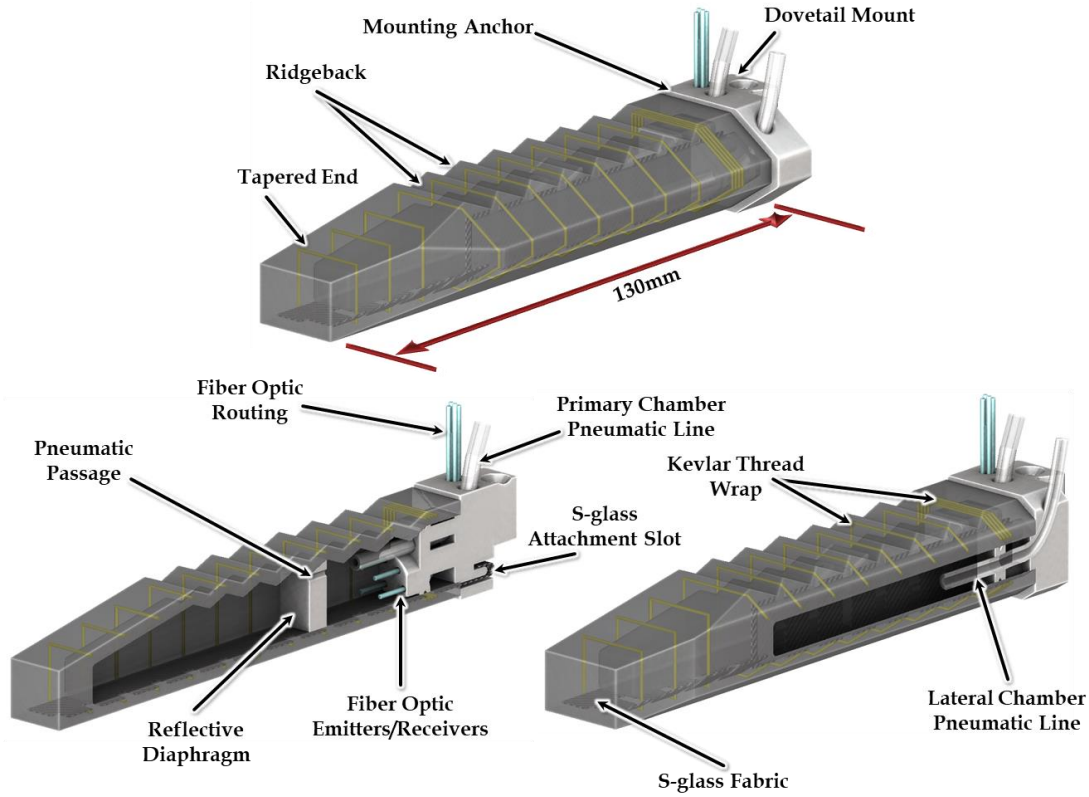

Figure 25- Claw Actuator with cross sectional views showing internal components in the primary and lateral chambers

A rough overall system outline was established for a prosthetic hand capable of grasping objects of daily living [32]. The device needed to display independent grasp function by means of soft actuation, and have capability for configurable digit positions to accommodate objects of broad form factor. Figure 24 displays the final system with the primary components labeled. The general premise was with 3 digits, two of which moving dexterously and one as palmar support. Coordinated motion in multiple planes established a demand for sensory feedback to monitor the state of the actuators. The designed actuators employ embedded sensing to add complex controller functionality of grasp synergies.

4.2.1 System Function

The authors' prior experience with actuator fabrication and design dictated that the dexterous actuator be of a fluidic elastic type with a woven fiber shell to induce longitudinal expansion along the primary axis [9, 33]. For dexterous control in multiple directions, multiple actuation chambers are necessary. Some bidirectional bending actuators achieve actuation by pressure differential in two chambers across a strain limiting neutral axis [23]. Each chamber allows for actuation in one direction through one plane. Deliberate design of the actuator body and placement of embedded components enabled asymmetrical actuation.

4.2.2 Mechanical Design of the Deformable Body

There are several aspects of the mechanical design that can be noted for facilitating deformation in the desired primary and lateral planes. Figure 25 shows the mechanical design features of the molded inflatable structure and embedded hardware.

The actuator body is composed of two chambers placed to prioritize bending in the primary direction followed by the lateral direction. The resulting structure for lateral actuation should minimally impede the structure for primary bending. This configuration can be seen in Figure 26 with the lateral mode of bending directed through the primary chamber. Equation 1 shows the fundamental equations for radius of curvature from a bending moment.

$$R = \frac{EI_x}{M_x} \tag{4}$$

$$I_x = \frac{xy^3}{12} \tag{5}$$

The radius of curvature, R, can be correlated to major bending when low and minor bending when high. Primary bending moment, M_x, is directly proportional to the internal pressure of the primary chamber. The moment of inertia about the primary bending axis, I_x, is dependent on the mechanical design of the cross section. By appending the second chamber laterally the added material increases I_x less than it would by adding the same material vertically in the y direction.

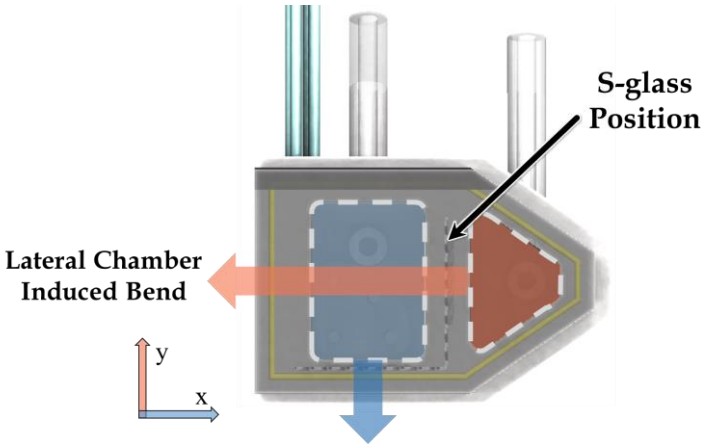

Figure 26- Cross section of claw actuator to demonstrate bending direction relative to chamber position.

The tapered end serves to increase stiffness at the cost of dynamic range in the distal region of the actuator. In this region, the overall cross section of the actuator decreases

while the wall thickness remains. This effectively increases the moment of inertia increasing stiffness and reducing bend for an induced moment. For grasping, this feature provides a larger normal force where it is anticipated to contact an object.

The ridgeback feature facilitates elongation of the chamber wall to which it is applied. It is applied to the chamber wall expected to experience the highest strain. By effectively adding material to disperse that strain, primary bending is facilitated.

The strain limiting s-glass layer was cut to be a solid bar under half of the primary chamber while segmented with spacing under the half adjacent to the lateral chamber. These segments were further bent vertically up between the two actuation chambers, as seen in Figure 26. The laser-cut shape, fabricated from a silicone encapsulated sheet of s-glass, is shown in Figure 27.

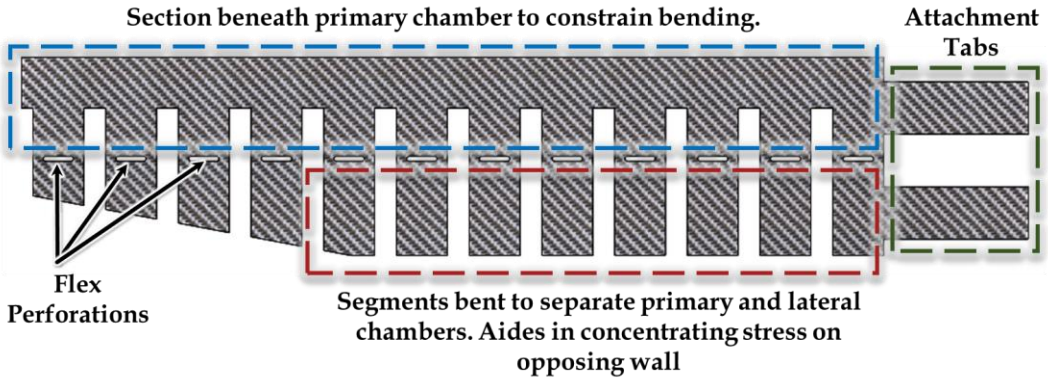

Figure 27- S-glass cutout for embedding as a strain limiting component in soft robots.

This SL component prioritizes primary bending while the segmented section allows lateral bending. Segments separating the chambers impede deformations between the two chambers, concentrating the induced forces at the ends.

4.2.3 Design of Reflective Diaphragm Sensor

The premise of the reflective diaphragm sensor is to measure changes in the amount of light reflected by a surface merged with the actuator body as it undergoes specific deformations. Similar in theory, extrinsic fiber optic force sensors for MRI catheters conduct this on a relatively smaller scale [34]. The arrangement of critical components for this sensor in the claw actuator is illustrated in Figure 28.

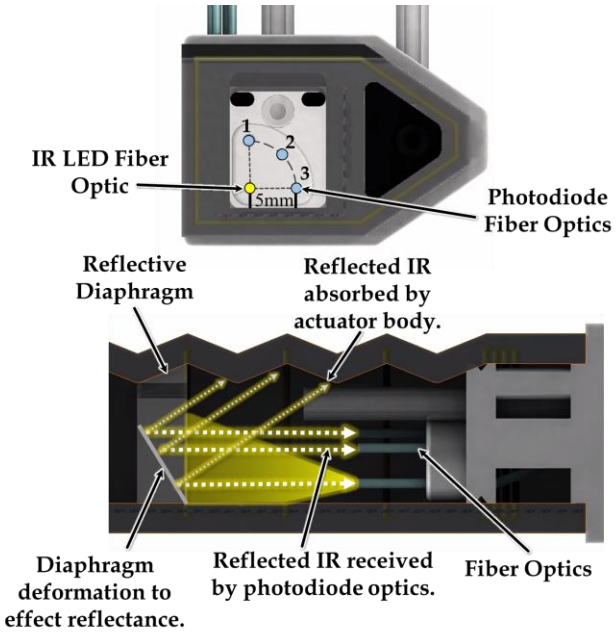

Figure 28- Actuator cross sections illustrating arrangement and interaction of components required for reflective diaphragm sensing

Four 1mm fiber optic cables are routed through the mounting anchor 8mm into the primary chamber. Orthogonal to the fiber optic array, a silicone diaphragm with opaque white pigment was molded 17mm from the fiber ends. The emitting fiber, connected to an IR LED, is placed closest to the neutral axis of the actuator, effectively above the solid portion of the SL layer. This placement is conducive to the emitter staying in axial line with the diaphragm through desired deformations.

Three fiber optic receivers, connected to IR photodiodes, are equidistant along a 5mm arc centered on the emitter. Light sensor one is placed, relative to the emitter, with orthogonal displacement from the primary bending plane. As the diaphragm follows the actuator body for primary bending, it will increase in angular displacement from vertical relative to the mount anchor. The displacement of light sensor one to the reflective diaphragm will increase most in these circumstances, and will hypothetically show the most sensitivity to primary bending. Similarly, light sensor three is hypothesized to show the highest sensitivity to lateral bending as it is placed, relative to the emitter, with orthogonal displacement to the lateral bending plane. Light sensor two, centered on the arc, serves as sensory information that helps in decoupling responses when used as a training feature in the appropriate modeling method.

4.2.4 Fabrication of Sensor Embedded Actuators

Materials used in building a claw for the AGA are as follows: S-glass fabric, Kevlar thread, 1mm fibre optic cable, three photodiodes (Industrial Fiber Optics; IF-D91), one IR diode (Industrial Fiber Optics; IF-E91D), silicone adhesive (Smooth-On, inc; Sil-Poxy), high strength epoxy (Loctite®; E-20HP) tygon tubing (1/8 inch OD, 1/16 inch ID), PLA 3D-printed components, silicone pigments (Smooth-On, inc; Silc Pig, black and white), and platinum cure silicones (Smooth-On, inc; Dragonskin 20, Dragonskin 10 NV, Ecoflex 50).

Fabrication of the actuators begins with the encapsulation of S-glass in a Dragonskin 10 NV. Silicone is poured over the fabric and pressed to remove excess silicone.

Encapsulation allows the sheet to be cut while maintaining structure of the fabric. The S-glass is then laser cut (Universal Laser Systems; PLS6.150D) to the desired shape of the strain limiting, SL, layer. The SL layer is then mated with the mold plug using a small amount of Ecoflex 50 as an adhesive, because of its rapid cure time and easy delamination from plastic. The plug assembly and stage one mold are then mated and injected with black pigmented Dragonskin 20. This Dragonskin, with shore hardnesss 20A, was determined to be of optimal stiffness through design revisions. The plug with first stage actuator is then demolded from stage one, and wrapped in Kevlar threading to prepare for stage two. The thread is aligned on the surface of the silicone by specific features molded by stage one, and fastened with Sil-Poxy. The actuator is then mated with stage two molds and filled with Dragonskin 10 NV, a silicone with a relatively low viscosity that can flow easily through any features or imperfections from the prior stage. Upon curing, stage two is demolded and the plug is removed from the actuator body. The actuator body is then fit onto a separate upright plug to mold the internal diaphragm. .5cc of white pigmented Ecoflex 50 is injected just above the diaphragm plug to mold a vented diaphragm of 5mm thick across the cross section of the primary chamber. The Actuator body is then removed from the diaphragm plug, ready to be mated with the fiber optic mount block assembly.

To prepare the mount block, the primary structure is 3D-printed (Fablicator, FDM) in PLA plastic. Tygon tube is then placed in the block so that 15mm will protrude into the chamber. Fiber optic cable is then routed through the block and into the anchor array so that 7mm will protrude into the chamber. The tube and fiber optics are then secured in the block with high strength epoxy. Upon the epoxy curing, the fiber optic mount block assembly is ready to be mated with the actuator body.

Mating the actuator block with the actuator body is done to ensure a secure seal of the chamber. The anchor of the mount block is coated with silicone adhesive and joined with the actuator body so that the body is flush with the block and the attachment tabs of the SL layer follow through the block. Attachment tabs are wrapped back into the block and fastened with silicone adhesive. The silicone adhesive provides a strong connection between the bodies, but does not ensure a pneumatic seal of the chamber. Dragonskin 10 NV is injected through the actuator body, into the anchor void to fill the gaps and provide a seal.

4.3 Evaluation of Reflective Diaphragm Sensors

To gauge the efficacy of reflective Diaphragm sensors, tests were conducted to illustrate the repeatability of sensor measurements, sensitivity within the range of operation, and the training of a system model. Ground truth for determining sensor performance was measured by electromagnetic trackers. These sensors were mounted at the tip of each actuator, Figure 29 below, and sampled to provide precise position at every reading of the actuator sensors.

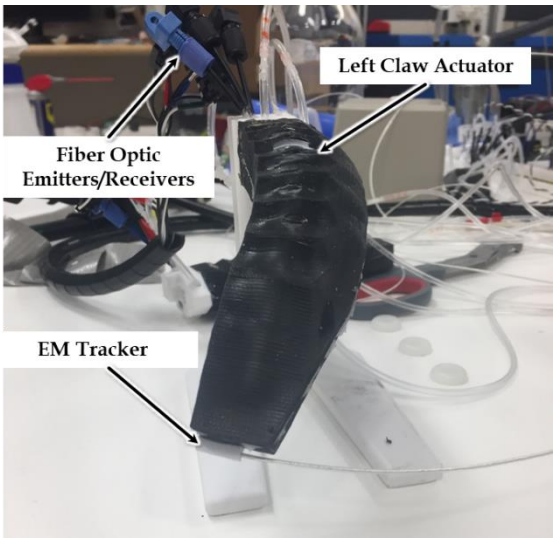

Figure 29-Left Claw actuator in flexion with EM tracker for ground truth measurement. The claw is clad in pigmented silicone to reject

4.3.1 Sensor Reliability

Sensors were first investigated for repeatability of measurements. The sensorized actuator was inflated to a primary pressure of 89.6 kPa for 10 cycles of 6 seconds each. As seen in Figure 30, all three sensor responses were repeatable over the full range of pressurization. Hysteretic behavior can likely be attributed to physical relaxation of the body. From statistical analysis on the cyclical testing, the signal to noise ratio for each sensor to primary bending was calculated. Sensor one, positioned for the highest sensitivity to primary bending had a signal to noise ratio of 33.52 db. Sensor two had a signal to noise ratio of 30.81 db. Sensor three, positioned for sensitivity to lateral actuation, had a signal to noise ratio of 21.86 db.

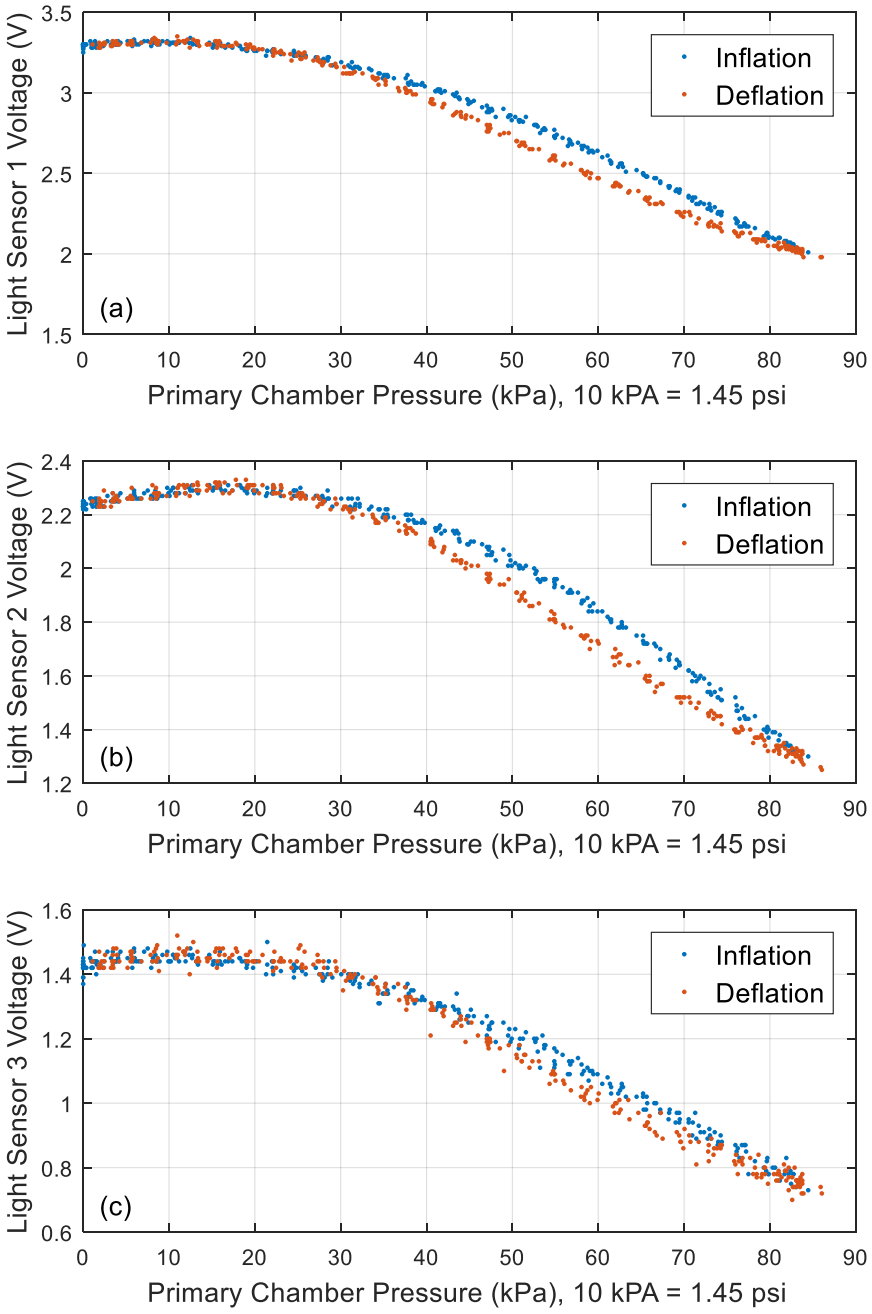

Figure 30- Light sensor voltages versus primary chamber pressure: (a) light sensor 1, (b) light sensor 2, (c) light sensor 3.

4.3.2 Sensitivity Analysis

A quality of interest for the sensors is their sensitivity to each physical input to the system. Testing the sensitivity was done by inflating the actuator through an array of all potential and safe configurations and observing the response at each. For actuator preservation, the array of test values ranged from 0 to 68.9 kPa for the primary chamber as well as the lateral chamber. The responses for each light sensor at every pressure configuration can be seen in Figure 31. As expected, light sensor one is exhibits the largest sensitivity to primary bending and the smallest to lateral while light sensor 3 exhibits the largest sensitivity to lateral bending. Each sensor shows a coupled response to each actuation mode.

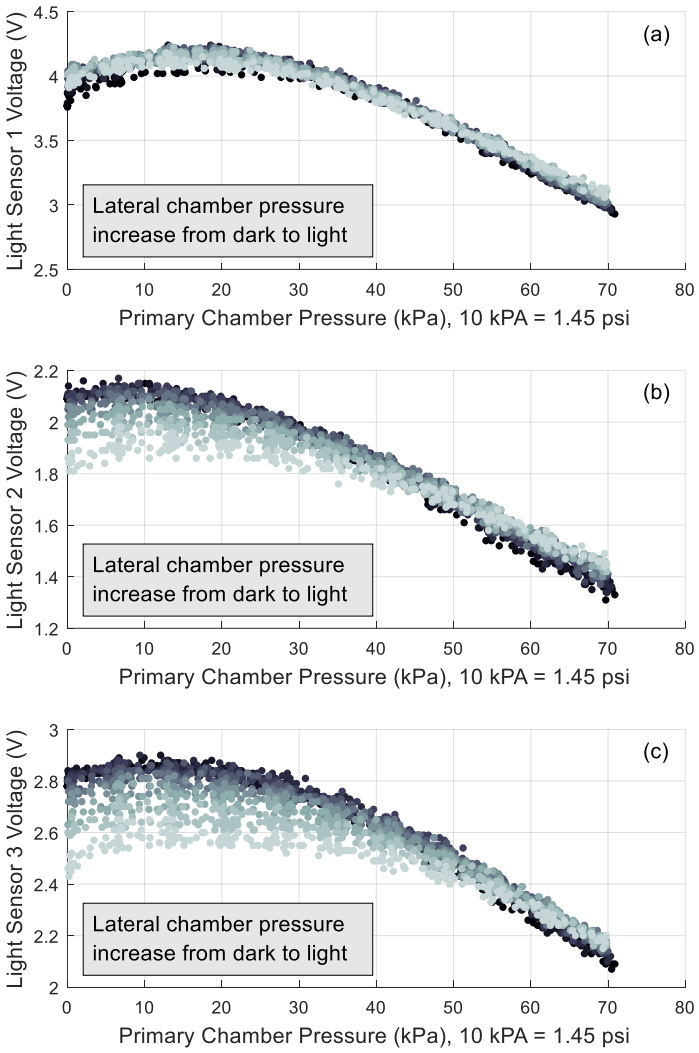

Figure 31- Light sensor voltages versus primary chamber pressure for varying lateral chamber pressures – lateral chamber pressure increases from dark to light data points: (a) light sensor 1, (b) light sensor 2, (c) light sensor 3.

4.3.3 Training the System Model

The objective of embedding sensors within the actuators is to ultimately use them as an estimate of actuator state in lieu of system modeling. To estimate claw tip displacement from light sensor data, a linear regression model was created for each claw via the sci-kit learn library in Python. Each of the three light sensor signals was specified

as a separate feature, while the horizontal, vertical, and backwards tip displacements of the claw – recorded via the EM tracker system – were specified as the training targets. Training data were scaled such that each feature vector had zero mean and unit variance.

The model was trained with light sensor and tip displacement data recorded over the full range of claw pressure configurations. Specifically, the claw primary chamber was gradually pressurized from 0 to 86.9 kPa and depressurized back to 0 kPa for constant lateral chamber pressures ranging from 0 to 62.1 kPa. Chamber pressures were ramped slowly to ensure that the claw remained in a quasi-static state throughout the pressurization sequence.

To evaluate the model, K-Folds cross-validation was performed with 3 folds. Data was first shuffled before being split. The root-mean-square error (RMSE) for horizontal, vertical, and backwards displacement predictions versus the corresponding targets were below 1.7 mm for all three test data sets. Figure 32 illustrates the trained model's ability to estimate tip position in 3-coordinates.

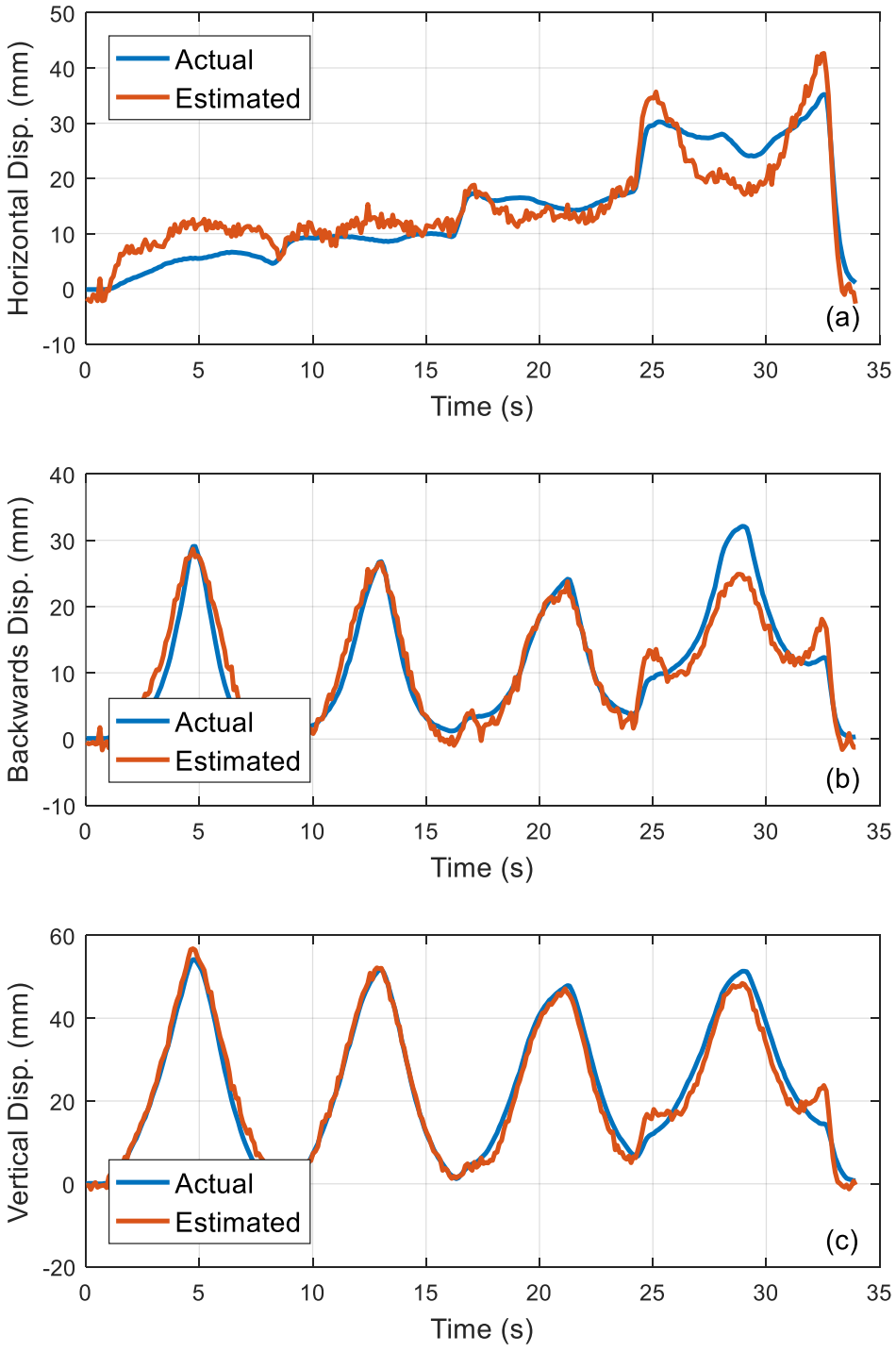

Figure 32- Claw tip displacement estimate versus actual for four primary chamber pressure cycles from 0 to 82.7 kPa, with respective lateral chamber pressures of 0

kPa, 20.7 kPa, 41.3 kPa, and 62.1 kPa: (a) horizontal displacement, (b) backwards displacement, (c) vertical displacement.

4.3.4 Signal Conditioning for System Potential

For system implementation it is necessary to quantify a reliable form of the sensor response for the controller. The base vertical tip displacement estimation was chosen for this purpose for its accuracy to ground truth and relative lack of noise. A derivation of the vertical displacement was taken to contrast the response for controller implementation. This derivation induced moderate noise that was smoothed by a moving average filter. The conditioned signal, seen in Figure 33, shows the conditioned estimation of vertical tip velocity for a free end actuator and actuator coming to contact with objects of different sizes.

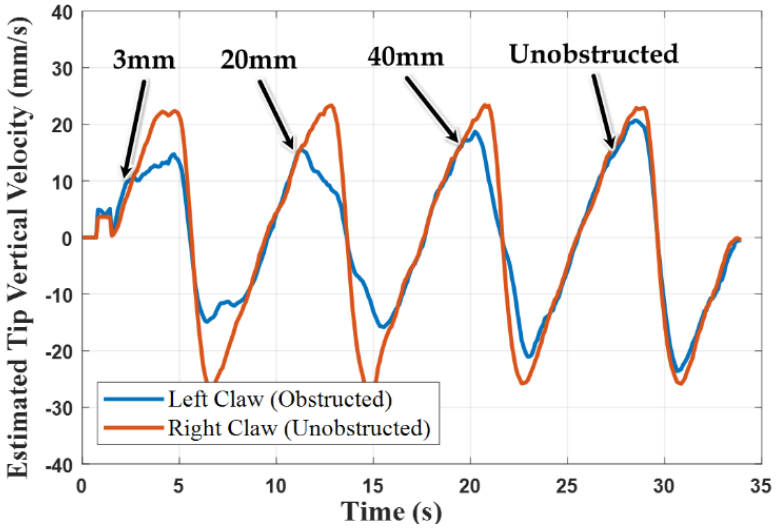

Figure 33- Estimated tip vertical velocity versus time for obstructed and unobstructed claws. Labeled peaks indicate displacement of tip before contact

4.4 Control of the Adaptive Grasp Appendage

The fully assembled device is composed numerous pneumatic chambers and various sensing technologies that all function in unison for system functionality. Each independent subsystem plays a critical role based on its mechanical design and how the integrated sensors inform its action within the control method. The control premise behind the system is designed to reduce cognitive load on the user. For the majority of its use, the AGA is operates passively, only changing in configuration when the user instructs it to do so. While operating, the device has the ability to adjust and compensate in grip passive from the user. In this fashion, we hope to facilitate patients from any degree of technological competency to orienting themselves to the device.

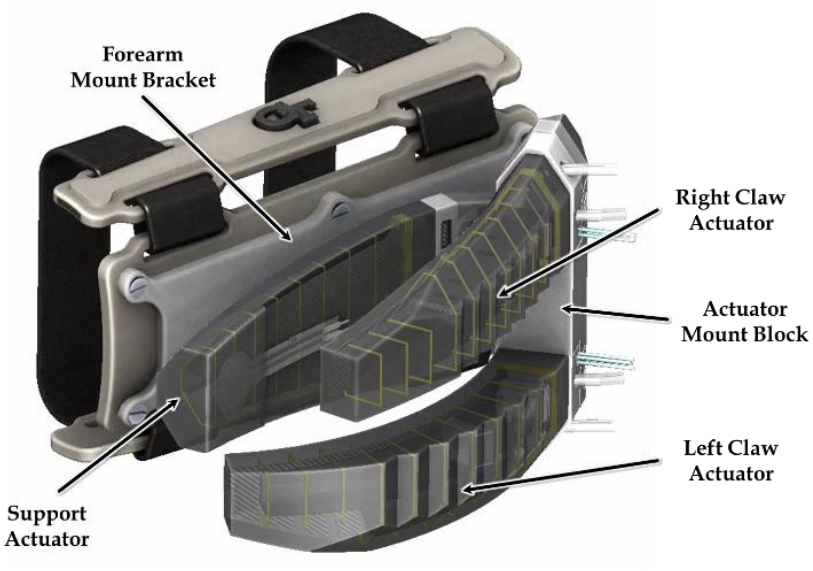

Figure 34- Render of AGA with primary components labeled.

4.4.1 Grasping Mechanism

The system operates with 3 soft actuators encompassing 6 independently inflatable chambers. The primary grasping digits operate distal to the users forearm. These digits are

mirrored about the central axis of the forearm in their actuation, and are responsible for dorsal bending as well as lateral pinching. The support digit operates proximal to the user's forearm. This actuator has the primary function of a relatively stiff palmer digit against which to grasp. Beyond the actuation mechanisms, the system is sensorized to provide internal feedback of position and grasp quality of each digit. Within the primary claw actuator, fiber optics are used reflectively to internal surfaces of the chamber to provide a dynamic response that can be correlated with a neural net. Further, the support actuator utilizes an FSR at its tip to characterize the grasp force and position on the object. The response from this sensor dictates the relative position of the primary claw digits to conform to an object of odd form. This combined system can be seen in Figure 34.

4.4.2 Design of Support Actuator

The primary function of the support actuator is to provide an opposing force similar to a palm as a stable grasping structure. This is enabled by several design features. The body of the support actuator drafts to a narrower width away from the mounting block while the chamber wall thickness remains the same. As described for the tapered claw tip, relative moment of inertia increases with the taper to inhibit flexion for increased stiffness at the induced moment. The base of the actuator is wider on the plane perpendicular to desired bending which increases the actuators resistance to lateral deformation. A truss separates the two chambers running lengthwise in the actuator to inhibit radial expansion and further increase actuator stiffness. An FSR at the tip was intended to compare desired grip force to actual grip force. With this iteration of the design, readings from the FSR were inconsistent with the expected model so the data was not utilized. This is likely due to the

sensor being molded in a soft medium that has potential to absorb force that would trigger a sensor response. A diagram of the actuator is seen in Figure 35.

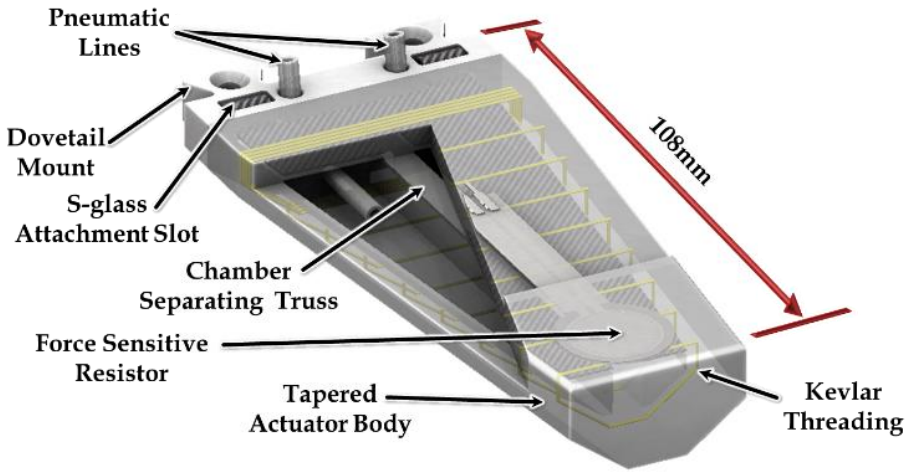

Figure 35- Support actuator diagram with cross section and primary design features labelled

4.4.3 Actuator Force Capabilities

Force capability of the claw actuators was collected for each independent plane of motion. For primary bending and lateral pinching the actuator was inflated from 0-103-0 kPa while making contact with the Instron load cell at the neutral 0 kPa. These results will be used to determine the ultimate grasping capability of the system.

The support actuator was placed into the Instron electromechanical test bed with the primary plane of motion through the crosshead, making neutral contact while at 0 kPa. The actuator was then inflated from 0-103 kPa with the force being recorded from the Instron. This force characterization was further used to infer the required internal pressure

required for the actuator. The force output vs internal pressure for each actuator is seen in Figure 36.

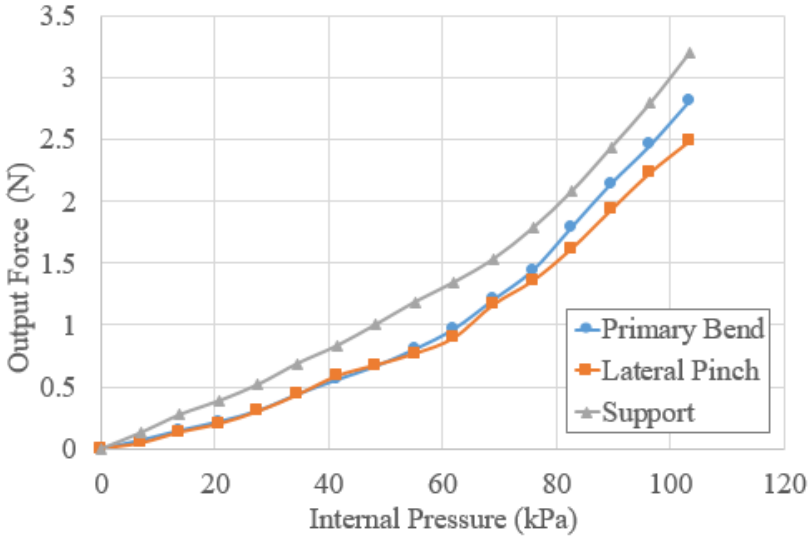

Figure 36- Force output against internal pressure for independent modes of actuation of the claw and support actuators

4.4.4 EMG Instrumentation

Surface Electromyographic (sEMG) signals are measured on the biceps and triceps from both arms by using the Myomo R&D EMG sensor. Each sensing unit is composed of two sensor heads with three electrodes on each head. The raw signals are recorded at a sampling rate of 1 KHz to avoid aliasing because the signal power of sEMG is predominantly within the range of 400-500 Hz [35]. The signals are full-wave rectified and processed with a high-pass filter (fc = 100 Hz) and a low-pass filter (fc = 3 Hz) to effectively remove the ambient noise from the power source and high frequency muscle contractions respectively.

4.4.5 Algorithmic Control of Actuators

The primary input is communicated through EMG signals from sensors located on each bicep. The EMG sensor located on the same side bicep as the device is responsible for controlling the primary bending of the device while the opposite side sensor is responsible for control of lateral flexion. Due to the coarse nature of the EMG signal recorded by raw skin contact, it was determined unsuitable to attempt reading specific intensity as a means of control. Instead, the length of the binary signal over a threshold was used as a more robust means of actuation. By taking the value of the EMG reading over a threshold as a value to be integrated over the duration of its hold, transient length can be used as a unidirectional input by which to operate the device. The visual representation of this can be seen in Figure 37.

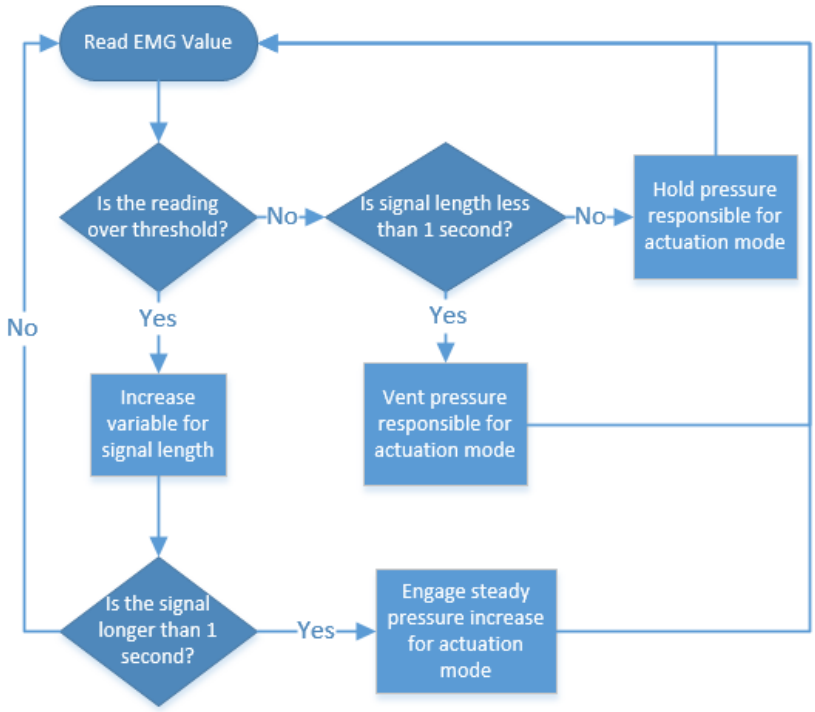

Figure 37 - Pseudocode for general pressure control algorithm from an EMG input

For the general interpretation of the EMG signal the decision was made to tie the function between pressure output and EMG input through the FSR array. For this process, the length of the EMG signal is being continuously mapped to a range of force outputs determined by the ultimate system capability. This mapping provides a desired value for force output that ramps so long as the EMG is held longer than .75s.

4.4.6 Pressure Control System

Actuation of the AGA device was achieved using a pneumatic control system to maintain each chamber of the robot at a desired pressure set-point. The control system used pulse-width modulation (PWM) of four SMC VQ100 Series solenoid valves to control airflow from a pressure source into the five chambers of the robot (Figure 38). The pressure source used was a Parker Hannifin BTC-IIS diaphragm pump connected to a 1-liter bottle

acting as a pressure accumulator chamber. The Soft Robotics Toolkit was used as a reference in selecting the aforementioned pump and valve components for the control system [3636].

A PID controller was implemented on an Arduino MEGA 2560 microcontroller to modulate the PWM duty cycle of each valve based on the corresponding pressure set-point value and pressure transducer measurement. The control input for each valve was updated at 10 Hz. To reduce pressure oscillations resulting from the binary on-off behavior of the solenoid valves, pneumatic damping was added to the system by placing a segment of 15-inch long, ½-inch inner diameter tubing between each valve and its respective pressure chamber. Additionally, pressure transducer data were sampled at 50 Hz and low-pass filtered via a 10^{th}-order finite-impulse response (FIR) filter with a cutoff frequency of 5 Hz.

In order to provide a relatively constant pressure source for the valve PWM control system, bang-bang control of the diaphragm pump was implemented on the Arduino, maintaining the accumulator chamber pressure between 14-16 psi. The Arduino microcontroller was also used to read all optical sensors connected inside the robot.

A Python script was used to update pressure set-point values on the Arduino microcontroller for each robot chamber at various time intervals, based on the aforementioned actuator control scheme. The script also recorded pressure transducer and optical sensor data from the Arduino, along with data from the ATC 3DGuidance trakSTAR electromagnetic (EM) tracker system used to measure the tip positions of the parallel claw actuators. All data was recorded at a 10 Hz sampling frequency.

Optical sensor leads were plugged into IR emitter and receiver housings at the base of the robot. The two IR emitters were powered in parallel using an external power supply of 6.6V and 0.07A.

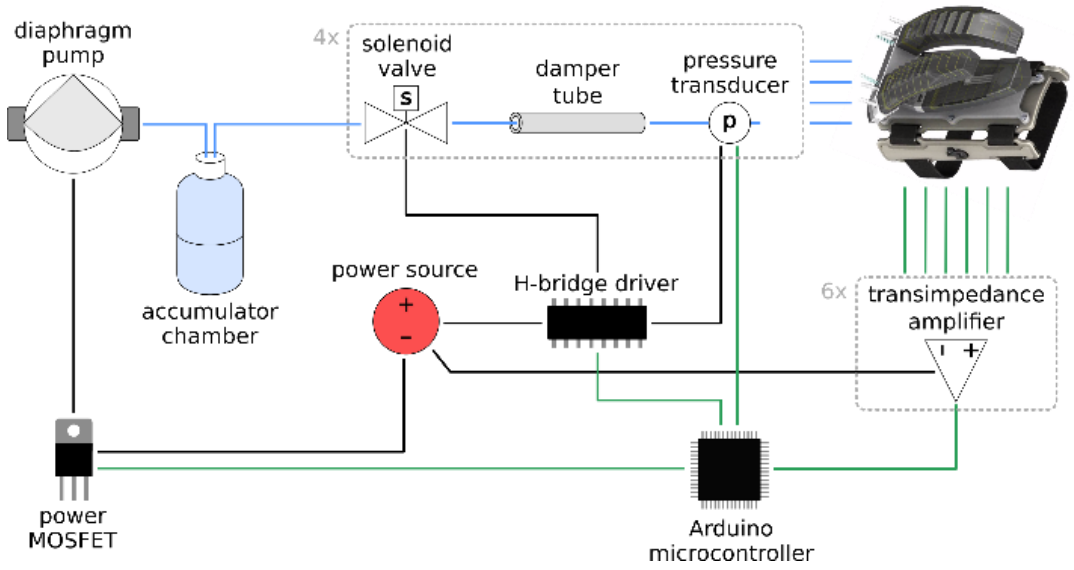

Figure 38- Soft robot pressure controller diagram; blue lines represent pneumatic connections, green lines represent signal connections, black lines represent power connections

4.4.7 Interference Detection through Positional Tracking

Having a system model trained from sensor data leads to the challenge of implementing the model in a control scheme. The model was trained to take inputs from the reflective diaphragm sensors to estimate an output of three coordinate tip position in free space. A time derivation of the vertical tip position is taken to find an estimation of velocity, more sensitive than position, and subsequent noise is filtered. When the actuator encounters an obstruction, the model interprets the change in velocity as an indication that the actuator has stopped moving and slows further pressurization of that digit until the other

digit makes contact with the object. Figure 39 illustrates the physical response of this controller where tracking of ground truth position for each actuator in collision can be seen impacting actuator pressurization.

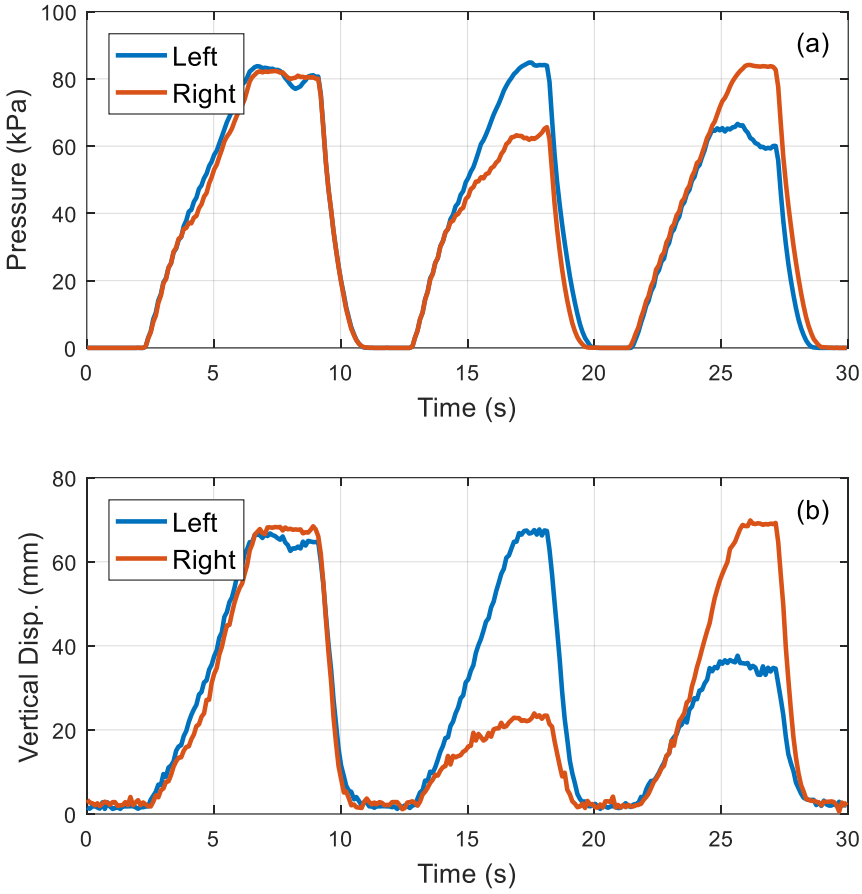

Figure 39- Plots of (a) pressurization of both claw actuators relative to (b) true tip position. Three cycles represent unobstructed actuation, right claw obstruction, and left claw obstruction respectively.

4.5 Application: Grasping Objects of Daily Living

The ultimate goal for the AGA is to enable grasp-ability for the user on the majority of objects they can expect to interact with on a daily basis [32]. A minimal mental load and maximum capability is desired for the user.

The primary capability of the AGA is its ability configure balanced grasp synergies autonomously. A set of objects to grasp was chosen to highlight this feature; a lightbulb, glasses, a drinking glass, a pear, a bag of chips, and a spool of wire.

4.5.1 System Performance

The AGA was tested in grasping all objects from the set with and without the collision detection feature. In general, the method of EMG input was intuitive and moderately robust. On occasion, motion of the left arm would register over the threshold and signal the release of grasping. As well, physical ingress of the device had potential to shift sensor baseline. Recalibration of the device was necessary after extended use.

4.5.2 Grasping Ability

The collision detection mechanism of the AGA was able to successfully modulate the primary pressure of each claw for grasp configuration. Whether or not this grasp configuration was optimal needs further investigation. From preliminary attempts at object grasping, it was evident that the configured grasp synergies did affect how the AGA grasped objects. Figure 40 shows the AGA in grasp of a pear with and without collision detection enabled in the controller.

The images indicate the actuators without collision detection in a state of potentially undesired deformation. Orientation of the tips appear twisted relative to the rest of the device. An observation from device operation was a tendency for the open loop ramp of the actuators to put extensive torque in the contacting actuator, often altering its position. Operation of the actuators with collision detection was perceived to help with grasping

objects with more contact force balance between the actuators. Although the device did not inherently fail at grasping any specific object, further investigation with grasp quality would likely show that the autonomous contact force balance would benefit the system.

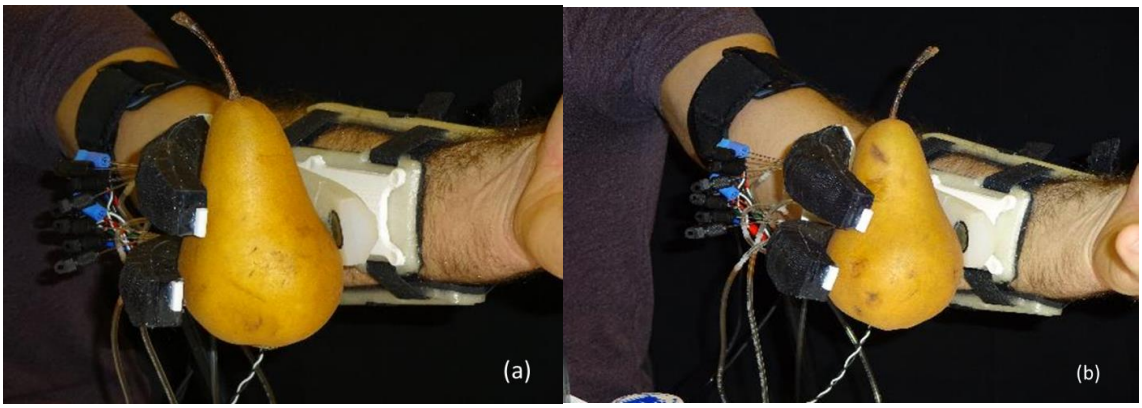

Figure 40- AGA in grasp of a pear (a) with collision detection and (b) without collision detection.

4.6 Discussion

The experimental evaluation of the reflective diaphragm sensors demonstrated that independent measurement of primary flexion and lateral bending motion in the soft pneumatic actuator were accurate to within 1.7 mm when a simple linear regression model. This result speaks to the fidelity of the proposed sensing technique and the promise of using the multiple sensors to decouple more complex deformations in other soft, pneumatic devices. The combination of reflective diaphragm sensor and pressure sensor data allowed the detection of contact events that would normally require the use of dedicated tactile sensors, indicating the reflective sensors may be combined with other sensing modalities to reduce implementation cost and mechanical design complexity – albeit at the expense of algorithmic/computational overhead.

Future research efforts will focus on the use of these sensors on devices with more complex deformation patterns, and the use of techniques like deep learning to measure both static and dynamic states of soft, pneumatically actuated devices.

CHAPTER 5. SUMMARY AND CONCLUSION

5.1 Conclusion

The task of integrating soft sensing technologies with soft actuation mechanisms proved complex. Upon fabricating actuators and actuators together it was realized that the sensor responses from the attempted methods are substantially coupled to the various actuator internal and external loading conditions. With sensors adapted to the supernumerary grasp assist, another unanticipated deformation of the actuator was likely linked to deviation of the response from predicted. Under internal pressurization of the chamber, the septum with aligned sensors underwent bowing away of the pressurized chamber yielding results inconsistent from the test septum. As investigated with object detection for the AGA, designing actuators with targeted kinematic sensing was able to substantially reduce the uncertainty in position under impeded motion of the actuator, yet to varying degrees for each plane of motion. The cause for this was potentially variable reflective parameters of the diaphragm under radial expansion of the actuator. Fortunately, by utilizing redundant sensors and a linear regression the responses were decoupled enough for practical application in the AGA.

5.2 Contribution for Soft Robotics

Primarily, this research makes an impact in how sensing is approached for soft robotic systems. The compliant nature of soft robots leads them to behave in physically unpredictable ways that may be detrimental to system performance. Striving for sensorized systems helps overcome this uncertainty by controlling through rudimental observation of the system. The research conducted during this phase specifically illustrates the performance of a novel sensing technique targeted to an actuator of unorthodox geometries

and bending modes. Specifically, reflective diaphragm sensors were implemented in actuators capable of motion in 2 independent planes to accurately characterize actuator tip position. Research also illustrates potential of analyzing the raw response of sensors to be utilized with machine learning even when an obvious correlation of responses cannot be seen.

In order for the field of soft robotics to expand, it needs to generate interest for practical applications. Development of complex systems is critical to outline the potential capabilities of soft robotics. The AGA utilizes techniques and design principles witnessed in research as ingredients to developing a rounded system of sensors and actuators. From a design perspective, this project outlines a process for developing a task specific soft robot with actuators and sensors working in harmony. In attempting to integrate sensors and soft actuators, insight is gained in the physical considerations that must be made in designing combined systems.

5.3 Future Work

There are improvements that can be made with the application of sensing to soft robotic systems. As these robotic systems become more complex, a demand for accuracy in soft robotic kinematic sensing will increase. With the general acclimation of soft robots to rapid fabrication and prototyping, the field would likely benefit from further investigation of redundant sensing for system training. This could involve the application of discrete sensors across an entire actuator and looking at specific groups of the sensors to optimize their placement.

With training, the actuators of the AGA were trained with a linear regression providing substantial accuracy to 1.7 mm of tip position. As well, this was performed as a quasi-static interpretation for training. Relative to many rigid mechanical actuators, these soft actuators are slow to respond due to the inherent damping of the elastic body. A study performing dynamic training on the actuators would describe the tradeoff between using dynamic testing conditions to the simple quasi-static method, and would help determine the level of training a system may demand for a specific application. Comparing the results from the linear regression to a more robust training method, potentially a nonlinear regression or a neural net, would also show what degree of accuracy each method is capable of, and again illustrate the cost-benefit relationship for methods of training.

REFERENCES

[1] C. D. Onal and D. Rus, "A modular approach to soft robots," in *Biomedical Robotics and Biomechatronics (BioRob), 2012 4th IEEE RAS & EMBS International Conference on*, 2012, pp. 1038-1045: IEEE.

[2] P. Polygerinos *et al.*, "Modeling of soft fiber-reinforced bending actuators," *IEEE Transactions on Robotics*, vol. 31, no. 3, pp. 778-789, 2015.

[3] K. Suzumori, S. Endo, T. Kanda, N. Kato, and H. Suzuki, "A bending pneumatic rubber actuator realizing soft-bodied manta swimming robot," in *Robotics and Automation, 2007 IEEE International Conference on*, 2007, pp. 4975-4980: IEEE.

[4] L. O. Tiziani, T. W. Cahoon, and F. L. Hammond, "Sensorized pneumatic muscle for force and stiffness control," in *Robotics and Automation (ICRA), 2017 IEEE International Conference on*, 2017, pp. 5545-5552: IEEE.

[5] R. E. Goldman, A. Bajo, and N. Simaan, "Compliant motion control for continuum robots with intrinsic actuation sensing," in *Robotics and Automation (ICRA), 2011 IEEE International Conference on*, 2011, pp. 1126-1132: IEEE.

[6] E. Rocon *et al.*, "Human-robot physical interaction," *Wearable Robots: Biomechatronic Exoskeletons*, pp. 127-163, 2008.

[7] C. Majidi, "Soft robotics: a perspective—current trends and prospects for the future," *Soft Robotics*, vol. 1, no. 1, pp. 5-11, 2014.

[8] M. T. Tolley *et al.*, "A resilient, untethered soft robot," *Soft Robotics*, vol. 1, no. 3, pp. 213-223, 2014.

[9] A. Hart, T. Cahoon, and F. L. Hammond III, "Measuring Multimodal Deformations in Soft Inflatable Actuators using Embedded Strain Sensors," presented at the IEEE International Symposium on Robot and Human Interactive Communication, RO-MAN 2017, Lisbon, Portugal, 2017.

[10] A. D. Marchese, C. D. Onal, and D. Rus, "Autonomous soft robotic fish capable of escape maneuvers using fluidic elastomer actuators," *Soft Robotics*, vol. 1, no. 1, pp. 75-87, 2014.

[11] Y.-L. Park, B.-R. Chen, and R. J. Wood, "Design and fabrication of soft artificial skin using embedded microchannels and liquid conductors," *IEEE Sensors Journal*, vol. 12, no. 8, pp. 2711-2718, 2012.

[12] J.-B. Chossat, Y.-L. Park, R. J. Wood, and V. Duchaine, "A soft strain sensor based on ionic and metal liquids," *IEEE Sensors Journal*, vol. 13, no. 9, pp. 3405-3414, 2013.

[13] D. M. Vogt, Y.-L. Park, and R. J. Wood, "Design and characterization of a soft multi-axis force sensor using embedded microfluidic channels," *IEEE Sensors Journal*, vol. 13, no. 10, pp. 4056-4064, 2013.

[14] R. K. Kramer, C. Majidi, R. Sahai, and R. J. Wood, "Soft curvature sensors for joint angle proprioception," in *Intelligent Robots and Systems (IROS), 2011 IEEE/RSJ International Conference on*, 2011, pp. 1919-1926: IEEE.

[15] F. L. Hammond, Y. Mengüç, and R. J. Wood, "Toward a modular soft sensor-embedded glove for human hand motion and tactile pressure measurement," in *Intelligent Robots and Systems (IROS 2014), 2014 IEEE/RSJ International Conference on*, 2014, pp. 4000-4007: IEEE.

[16] F. Caralt, J. Molnar, T. Cahoon, J. Stingel, and F. L. Hammond, "Diffusion-Based Optical Sensors for Multimodal Strain Measurement in Soft Devices," presented at the IEEE Sensor Conference, Glasgow, Scotland, UK, 2017.

[17] C. To, T. L. Hellebrekers, and Y.-L. Park, "Highly stretchable optical sensors for pressure, strain, and curvature measurement," in *Intelligent Robots and Systems (IROS), 2015 IEEE/RSJ International Conference on*, 2015, pp. 5898-5903: IEEE.

[18] L. Jiang, K. Low, J. Costa, R. J. Black, and P. Yong-Lae, "Fiber Optically Sensorized Multi-fingered Robotic Hand," *IEEE International Conference on Intelligent Robots and Systems (IROS)*, 2015.

[19] L. Tiziani, A. Hart, T. Cahoon, F. Wu, H. H. Asada, and F. L. Hammond, "Empirical characterization of modular variable stiffness inflatable structures for supernumerary grasp-assist devices," *The International Journal of Robotics Research*, p. 0278364917714062, 2017.

[20] S. Seok, C. D. Onal, K.-J. Cho, R. J. Wood, D. Rus, and S. Kim, "Meshworm: a peristaltic soft robot with antagonistic nickel titanium coil actuators," *IEEE/ASME Transactions on mechatronics*, vol. 18, no. 5, pp. 1485-1497, 2013.

[21] F. L. Hammond, F. Y. Wu, and H. H. Asada, "Variable stiffness pneumatic structures for wearable supernumerary robotic devices," in *International Symposium on Robotics Research*, Sestri Levanta, Italy, 2015.

[22] K. C. Galloway, P. Polygerinos, C. J. Walsh, and R. J. Wood, "Mechanically programmable bend radius for fiber-reinforced soft actuators," in *Advanced Robotics (ICAR), 2013 16th International Conference on*, 2013, pp. 1-6: IEEE.

[23] F. L. Hammond III, F. Wu, and H. H. Asada, "Variable stiffness pneumatic structures for wearable supernumerary robotic devices," in *Robotics Research*: Springer, 2018, pp. 201-217.

[24] P. Polygerinos, Z. Wang, K. C. Galloway, R. J. Wood, and C. J. Walsh, "Soft robotic glove for combined assistance and at-home rehabilitation," *Robotics and Autonomous Systems,* vol. 73, pp. 135-143, 2015.

[25] P. Polygerinos *et al.*, "Towards a soft pneumatic glove for hand rehabilitation," in *Intelligent Robots and Systems (IROS), 2013 IEEE/RSJ International Conference on*, 2013, pp. 1512-1517: IEEE.

[26] T. Giffney *et al.*, "Soft pneumatic bending actuator with integrated carbon nanotube displacement sensor," *Robotics,* vol. 5, no. 1, p. 7, 2016.

[27] R. Deimel and O. Brock, "A novel type of compliant and underactuated robotic hand for dexterous grasping," *The International Journal of Robotics Research,* vol. 35, no. 1-3, pp. 161-185, 2016.

[28] R. K. Kramer, C. Majidi, and R. J. Wood, "Wearable tactile keypad with stretchable artificial skin," in *Robotics and Automation (ICRA), 2011 IEEE International Conference on*, 2011, pp. 1103-1107: IEEE.

[29] H. Zhao, K. O'Brien, S. Li, and R. F. Shepherd, "Optoelectronically innervated soft prosthetic hand via stretchable optical waveguides," *Science Robotics,* vol. 1, no. 1, p. eaai7529, 2016.

[30] M. K. Dobrzynski, R. Pericet-Camara, and D. Floreano, "Contactless deflection sensor for soft robots," in *Intelligent Robots and Systems (IROS), 2011 IEEE/RSJ International Conference on*, 2011, pp. 1913-1918: IEEE.

[31] I. Hussain, G. Salvietti, G. Spagnoletti, and D. Prattichizzo, "The soft-sixthfinger: a wearable emg controlled robotic extra-finger for grasp compensation in chronic stroke patients," *IEEE Robotics and Automation Letters,* vol. 1, no. 2, pp. 1000-1006, 2016.

[32] K. Matheus and A. M. Dollar, "Benchmarking grasping and manipulation: Properties of the objects of daily living," in *Intelligent Robots and Systems (IROS), 2010 IEEE/RSJ International Conference on*, 2010, pp. 5020-5027: IEEE.

[33] D. Rus and M. T. Tolley, "Design, fabrication and control of soft robots," *Nature,* vol. 521, no. 7553, pp. 467-75, May 28 2015.

[34] P. Polygerinos, T. Schaeffter, L. Seneviratne, and K. Althoefer, "A fibre-optic catheter-tip force sensor with MRI compatibility: A feasibility study," in *Engineering in Medicine and Biology Society, 2009. EMBC 2009. Annual International Conference of the IEEE*, 2009, pp. 1501-1054: IEEE.

[35] E. A. Clancy, E. L. Morin, and R. Merletti, "Sampling, noise-reduction and amplitude estimation issues in surface electromyography," *Journal of Electromyography and Kinesiology,* vol. 12, no. 1, pp. 1-16, 2002.

[36] D. P. Holland, E. J. Park, P. Polygerinos, G. J. Bennett, and C. J. Walsh, "The soft robotics toolkit: shared resources for research and design," *Soft Robotics*, vol. 1, no. 3, pp. 224-230, 2014.